Stem Cell Reports
Article

ISSCR

OPEN ACCESS

Age-related pathological impairments in directly reprogrammed dopaminergic neurons derived from patients with idiopathic Parkinson's disease

Janelle Drouin-Ouellet,[1,6,*] Emilie M. Legault,[1,6] Fredrik Nilsson,[2] Karolina Pircs,[2] Julie Bouquety,[1] Florence Petit,[1] Shelby Shrigley,[2] Marcella Birtele,[2] Maria Pereira,[2] Petter Storm,[2] Yogita Sharma,[2] Andreas Bruzelius,[2] Romina Vuono,[3,4] Malin Kele,[5] Thomas B. Stoker,[3] Daniella Rylander Ottosson,[2] Anna Falk,[5] Johan Jakobsson,[2] Roger A. Barker,[3] and Malin Parmar[2,*]

[1]Faculty of Pharmacy, Université de Montréal, Montreal, QC H3T 1J4, Canada
[2]Department of Experimental Medical Science, Wallenberg Neuroscience Center, Division of Neurobiology and Lund Stem Cell Center, Lund University, BMC A11 and B10, S-221 84 Lund, Sweden
[3]Wellcome-MRC Cambridge Stem Cell Institute & John van Geest Centre for Brain Repair, Department of Clinical Neurosciences, University of Cambridge, Forvie Site, Cambridge CB2 0PY, UK
[4]Medway School of Pharmacy, University of Kent, Chatham Maritime, Chatham ME4 4TB, UK
[5]Department of Neuroscience, Karolinska institutet, Stockholm, Sweden
[6]These authors contributed equally
*Correspondence: janelle.drouin-ouellet@umontreal.ca (J.D.-O.), malin.parmar@med.lu.se (M.P.)
https://doi.org/10.1016/j.stemcr.2022.08.010

SUMMARY

We have developed an efficient approach to generate functional induced dopaminergic (DA) neurons from adult human dermal fibroblasts. When performing DA neuronal conversion of patient fibroblasts with idiopathic Parkinson's disease (PD), we could specifically detect disease-relevant pathology in these cells. We show that the patient-derived neurons maintain age-related properties of the donor and exhibit lower basal chaperone-mediated autophagy compared with healthy donors. Furthermore, stress-induced autophagy resulted in an age-dependent accumulation of macroautophagic structures. Finally, we show that these impairments in patient-derived DA neurons leads to an accumulation of phosphorylated alpha-synuclein, the classical hallmark of PD pathology. This pathological phenotype is absent in neurons generated from induced pluripotent stem cells from the same patients. Taken together, our results show that direct neural reprogramming can be used for obtaining patient-derived DA neurons, which uniquely function as a cellular model to study age-related pathology relevant to idiopathic PD.

INTRODUCTION

Parkinson's disease (PD) is a neurodegenerative disorder that has a major pathology within the midbrain dopaminergic (DA) neurons and involves the aggregation of the misfolded protein alpha-synuclein (αSYN). How the disease arises and develops is currently unknown and no cure exists. There is an urgent need for better treatments and disease modifying therapies, but their development is hampered by a poor understanding of the pathogenesis of PD and lack of appropriate model systems, in particular ones that capture age, the biggest risk factor for developing this condition.

To better recapitulate disease relevant features and age, we have established a protocol for making induced neurons (iNs) that can be directly generated from adult human dermal fibroblasts (aHDFs). This type of direct neural conversion offers several advantages. In particular, such cells retain many important aspects of the aging signatures of the starting fibroblasts, including age-related changes in the epigenetic clock, the transcriptome and microRNAs, the reactive oxygen species level, DNA damage and telomeres length, as well as in their metabolic profile and mitochondrial defects (Huh et al., 2016; Kim et al., 2018; Mertens et al., 2015, 2021; Tang et al., 2017).

The idiopathic nature of most PD cases, coupled to the late age at onset, complicates the study of pathophysiology as it is challenging to design and interpret models of idiopathic PD. For example, animal models depend on toxin-induced mitochondrial damage or overexpression of αSYN at non-physiological levels (i.e., levels that exceed what is observed in idiopathic PD patients). Patient-derived induced pluripotent stem cells (iPSCs) are frequently used to study cellular features of PD (Brazdis et al., 2020; Lang et al., 2019) but fail to capture the age and epigenetic signatures of the patient (Lapasset et al., 2011; Mertens et al., 2015, 2021; Miller et al., 2013; Tang et al., 2017).

In this study, we investigated iNs using specific combinations of transcription factors and fate determinants without a pluripotent intermediate (Ambasudhan et al., 2011) as a mean to better recapitulate disease-relevant features of idiopathic PD. While it is possible to generate iNs with a DA-like phenotype (Caiazzo et al., 2011; Jiang et al., 2015; Li et al., 2019; Pereira et al., 2014; Pfisterer et al., 2011), current protocols are not efficient enough to

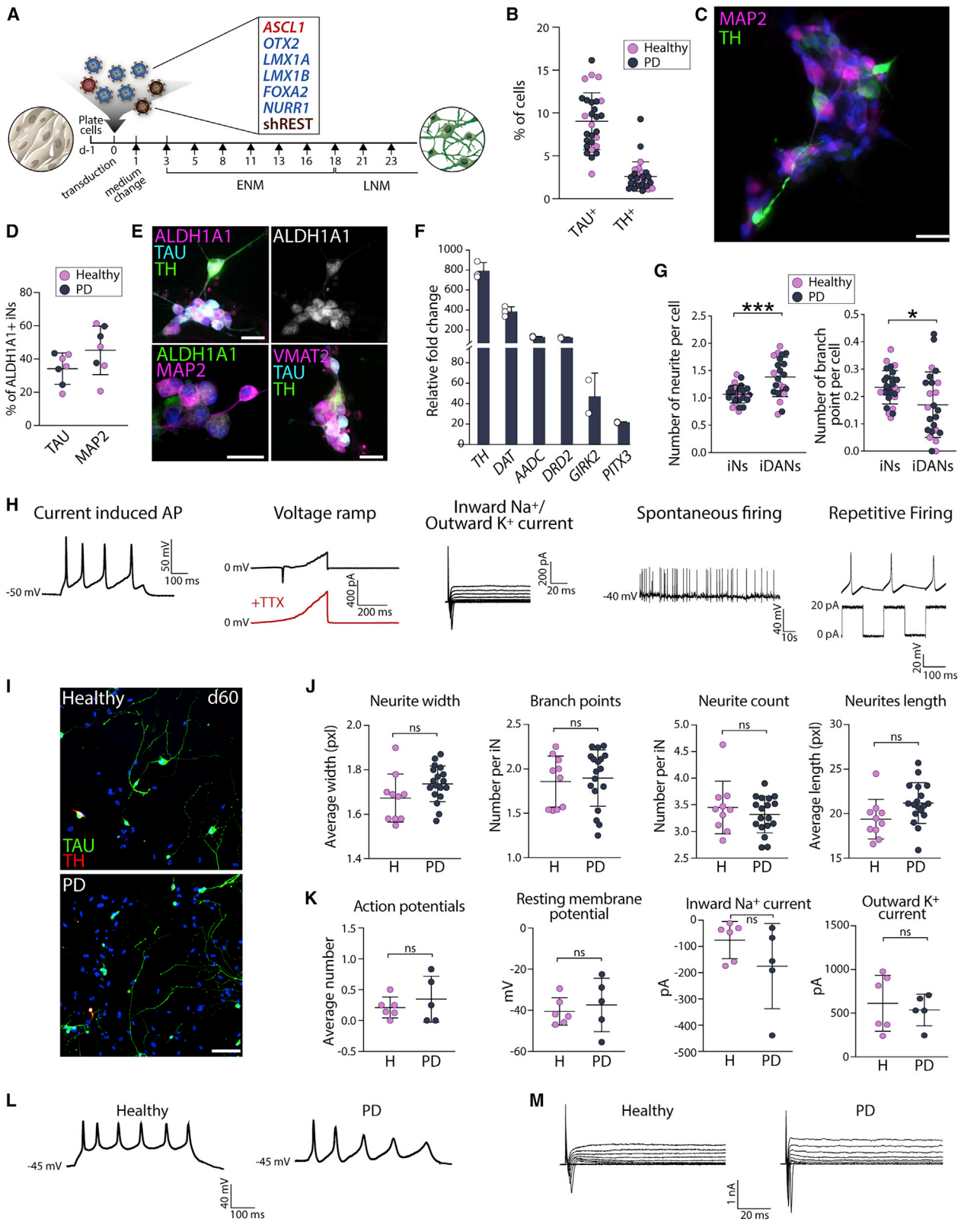

(legend on next page)

generate DA neurons from aHDFs of elderly donors in numbers required for further downstream experimental studies. Therefore, we first identified a combination of reprogramming factors that resulted in the efficient generation of subtype-specific and functional induced DA neurons (iDANs) when converting aHDFs from aged individuals. Subsequently, we used this protocol to convert iDANs from idiopathic PD patient-derived aHDFs as well as age- and sex-matched controls.

When analyzing the patient-derived neurons, we found stress-induced chaperone-mediated autophagy (CMA) and macroautophagy impairments in the idiopathic PD iNs but not in control iNs or in parental aHDFs of the patients. This type of pathology has previously only been captured in genetic PD variants using iPSC-based models (Sánchez-Danés et al., 2012; Schöndorf et al., 2014), and we hypothesized that the ability to do so in idiopathic PD iNs as reported here is related to maintenance of donor age in the iNs. To test this, we established iPSCs from a subset of the same patients. This analysis confirmed that fibroblast-derived iNs maintain expression of age-associated genes and express mature isoforms of TAU (4R), whereas iPSC-derived iNs do not. In line with this, we were able to detect αSYN pathology in directly converted patient-derived neurons but not in iPSC-generated patient-derived neurons. This study thus reports PD-associated phenotypes in directly converted neurons from patient aHDFs and provides a new model to study idiopathic forms of PD.

RESULTS

Generation of functional iDANs from aHDFs of adult donors

To enable a cell-based model of idiopathic PD using iNs with characteristics of aged DA neurons, we screened 10 different reprogramming factors (*Ascl1*, *Lmx1a*, *Lmx1b*, *Foxa2*, *Otx2*, *Nr4a2* (*Nurr1*), *SMARCA1*, *CNPY1*, *EN1*, *PAX8*) that were selected based on their (1) role during normal DA neurogenesis (Luo and Huang, 2016), (2) expression in the normal human fetal ventral midbrain (Nelander et al., 2013), (3) value in predicting functional DA differentiation from hPSCs (Kirkeby et al., 2017), and/or (4) role on midbrain-specific chromatin modeling (Metzakopian et al., 2015). All factors were expressed in combination with the knockdown of the RE1-silencing transcription factor (*REST*) according to our published protocol for high efficiency reprograming of aHDFs (Drouin-Ouellet et al., 2017). Three of the screened combinations gave rise to a significant proportion of tyrosine hydroxylase (TH)-expressing neurons: sh*REST*, *Ascl1*, *Lmx1a*, *Lmx1b*, *Foxa2*, *Otx2* (2.21% ± 2.02), sh*REST*, *Ascl1*, *Lmx1a*, *Lmx1b*, *Foxa2*, *Otx2*, *SMARCA1* (7.50% ± 3.55%), and sh*REST*, *Ascl1*, *Lmx1a*, *Lmx1b*, *Foxa2*, *Otx2*, *Nr4a2* (Figures 1A and S1A). The best TH-positive cell yield was obtained with the last combination, which gave rise to up to 70.3% ± 0.3% of cells expressing the neuronal marker TAU, of which 16.1% ± 2.01% also expressed TH (Figure S1A),

Figure 1. Generation of iDANs from Parkinson's disease and heathy donor lines

(A) Reprogramming iDANs from adult fibroblasts.

(B) Quantification of TAU-positive and TH-positive cells (mean average of 2,575 TAU-positive and 32 TH-positive cells assessed per line, n = 28 lines). Data are expressed as mean ± the SD.

(C) TAU-positive and TH-positive iDANs. Cells are counterstained with DAPI (in blue). Scale bar, 25 μm.

(D) Quantification of ALDH1A1 and TAU or MAP2 double-positive cells (mean average of 1,652 TAU-positive and 1,258 MAP2-positive cells assessed per well from four replicates per line, n = 7 lines (lines #4, #8, #9, #10, #26, #27, and #28). Data are expressed as mean ± the SD.

(E) TAU-positive, MAP2-positive, and TH-positive iNs and iDANs expressing ALDH1A1 and VMAT2. Cells are counterstained with DAPI (in blue). Scale bars, 25 μm.

(F) Gene expression quantification of DA genes relative to parental fibroblast levels (from two to three well replicates [white dots] from line #2). Data are expressed as mean ± the SD.

(G) Quantification of the neurite profile in TAU-positive and TH-negative (iNs) versus TAU and TH double-positive cells (iDANs) from healthy and Parkinson's disease lines (mean average of 2,575 TAU-positive and 32 TH-positive cells assessed per line, n = 28 lines). Two-tailed unpaired t test with Welch's correction: ***p = 0.0004, df = 30.82; *p = 0.0245, df = 32.94. Data are expressed as mean ± the SD.

(H) Patch clamp recordings of iDANs from line #2 (at day 65).

(I) Double TAU-positive and TH-positive H-iDANs and PD-iDANs at day 60. Scale bar, 100 μm.

(J) Quantification of the neurite profile in TAU-positive H-iNs and PD-iNs (experiment has been repeated independently three times, mean average of 2,142 TAU-positive cells assessed per line, n = 10 healthy and n = 18 Parkinson's disease lines). Data are expressed as mean ± the SD.

(K) Quantification of voltage-clamp recordings of evoked action potentials (n = 8–10 neurons per line, n = 5–6 lines per group), resting membrane potential of H-iNs and PD-iNs (n = 4–9 neurons per line, n = 5–6 lines per group), inward and outward currents (n = 4–9 neurons per line, n = 5–6 lines per group). Lines #1, #2, #4, #5, #6, #8, #13, #16, #17, #24, #28 were used for patch clamp experiments. Data are expressed as mean ± the SD.

(L) Voltage-clamp recordings of repetitive evoked action potentials.

(M) Representative traces of membrane sodium and potassium currents following voltage depolarization steps in H-iNs and PD-iNs. APs, action potentials; ns, not significant; TTX, tetrodotoxin.

with an average TAU purity of 9.1% ± 3.3% and TH purity of 2.6% ± 1.7% (Figures 1B and 1C) when reprogramming all lines used in the study (see Table 1), and showed robust upregulation of DA genes as measured by RT-qPCR (Figure S1B).

Further characterization of the iNs obtained using this reprogramming factor combination showed that, in addition to TH, 35.38% ± 9.05% of the TAU-positive and 45.20% ± 14.65% of the MAP2-positive cells were also expressing ALDH1A1 (Figure 1D), which is found in a subset of A9 DA neurons that are more vulnerable to loss in PD (Poulin et al., 2014), as well as VMAT2, a key DA neuronal marker (Figure 1E). Gene expression profiling of 76 neuronal genes relating to dopaminergic, glutamatergic, and GABAergic neuronal subtypes confirmed an upregulation of key genes related to DA patterning and identity (*FOXA1*, *OTX1*, *SHH*, *PITX3*), as well as DA synaptic function, including the receptors *DRD1* to *DRD5*; the DA transporter *SLC6A3* (*DAT*); the enzymes *DDC*, *MAOA*, and *ALDH1A1*; and the A9-enriched DA marker *KCNJ6* (*GIRK2*) (Figures 1F, S1C, and S1D). Thus the iDANs expressed the key markers of the AT-DAT^{high} subgroup of the DA sublineage as identified in Tiklová et al. (2019). Finally, to get a better idea of the identity of the cells that did not convert to iNs, we performed a triple staining using MAP2 to identify iNs, as well as GFAP and collagen 1 to identify potential glial cells and cells that remained fibroblasts. We observed that some MAP2-negative cells are expressing either collagen 1 or GFAP alone, or together (Figure S1E).

Morphologically, the iNs are quite immature at this stage (i.e., day 25–30), but high-throughput image acquisition analysis showed that TH-positive iNs express significantly more neurites compared with non-TH iNs but had significantly fewer branch points (Figure 1G). Patch-clamp electrophysiological recordings 65 days post transduction confirmed that the reprogrammed cells had functionally matured (Figure 1H). They were able to fire repetitive action potentials upon injection of current as well as exhibited inward-sodium, outward-potassium currents with depolarizing steps. When a continuous depolarizing voltage ramp was applied, inward currents were seen across the membrane and could be blocked by the neurotoxin tetrodotoxin, indicating an involvement of voltage-gated sodium channels in these currents. Without any injection of current or voltage, the cells displayed spontaneous firing, and 43.8% of iNs also showed rebound action potentials and/or pacemaker-like activity typical of mesencephalic DA neurons (Figure 1H). Based on this, we refer to the cells as iDANs.

Generation of functional iDANs from aHDFs of idiopathic Parkinson's disease patients

Using this new iDAN reprogramming method, we next converted aHDFs of 18 idiopathic PD patients and 10 age- and sex-matched healthy donors (Table 1). We found that the aHDFs obtained from PD patients reprogrammed at a similar efficiency to those obtained from healthy donors (Figure 1B) and displayed a similar neuronal morphological profile (Figures 1I and 1J). When measuring their functional properties using patch clamp electrophysiological recordings, we confirmed that iNs derived from healthy donors (H-iNs) and from PD patients (PD-iNs) displayed similar functionalities in terms of the number of current-induced action potentials, resting membrane potential, and the inward-sodium, outward-potassium currents (Figures 1K–1M).

PD-iDANs show altered chaperone-mediated autophagy

To assess the presence of age- and PD-related pathological impairments in iDANs derived from idiopathic PD patients, we focused on autophagy, a lysosomal degradation pathway that is important in cellular homeostasis and the efficiency of which decreases with age (Rubinsztein et al., 2011). We first looked for CMA alterations as this is one type of autophagy that has been suggested to be implicated in the pathophysiology of PD (Cuervo et al., 2004). During CMA, HSC70 recognizes soluble proteins carrying a KFERQ-like motif and guides them to the transmembrane LAMP2a receptor. Thereafter, the protein cargo is translocated into the lysosomal lumen and, as such, the level of LAMP2a determines the rate of CMA (Klionsky et al., 2016). To induce autophagy, cells were cultured under starvation conditions, which promotes the recycling of non-essential proteins and organelles for reuse (Klionsky et al., 2016). After validating that the starvation regimen had no impact on the number of neurons and induced changes in LAMP2a and HSC70 expression using western blot (WB) (Figures S2A–S2C), we assessed CMA expression using a high-content imaging approach, which allowed us to analyze cytoplasmic puncta in parental aHDFs, iNs (TAU positive and TH negative), and iDANs (TAU positive and TH positive) in a quantitative manner, and also to determine their subcellular location. When investigating this in parental aHDFs and PD-iNs at baseline and in the context of starvation using an antibody specific to the "a" isoform of LAMP2, we observed a slight reduction in LAMP2a-positive cytoplasmic puncta in healthy donors' parental aHDFs, which was also seen in PD patients' aHDFs, although this was not significant (Figures S2F and S2G). Moreover, we did not observe a difference in LAMP2a-positive cytoplasmic puncta in the neurites of TAU-positive iNs upon starvation in both H-iNs and PD-iNs (Figures S2J and S2K). However, when looking specifically at iDANs, we observed a lower number of LAMP2a-positive cytoplasmic puncta in the neurites at baseline in the PD-iDANs compared with H-iDANs, suggesting a lower

Table 1. Demographics, clinical, and genotype data of the study participants

Line ID	Group	Sex	Age at biopsy	MAPT haplotype	Age at onset (years)	Disease duration (years)	[a]UPDRS motor decline	[a]MMSE score decline	iPSC lines
1	healthy	M	69	H1/H1					
2	healthy	F	67	H1/H1					
3	healthy	M	80	H2/H2					
4	healthy	F	75	H1/H1					healthy 4
5	healthy	M	70	H1/H2					healthy 5
6	healthy	F	70	H1/H2					
7	healthy	M	71	H1/H1					
8	healthy	F	61	H1/H2					healthy 8
9	healthy	F	66	H2/H2					
10	healthy	F	58	H1/H1					
	ratio F:M/ mean ± SD	6:4	68.7 ± 6.3						
11	PD	M	56	H1/H1	34	23	−0.32	0	
12	PD	M	60	H1/H1	48	12	−0.43	0	
13	PD	F	77	H2/H2	65	12	1.48	0	
14	PD	F	67	H1/H1	56	12	0.76	−0.07	
15	PD	F	59	H1/H1	45	15	−1.39	0	
16	PD	F	80	H1/H2	69	11	0.39	−0.07	
17	PD	M	80	H2/H2	49	33	1.70	0	
18	PD	F	87	H1/H1	72	15	0.25	−0.12	
19	PD	F	77	H1/H1	56	24	−0.42	−0.25	
20	PD	M	75	H1/H1	63	13	−1.18	0	
21	PD	M	77	H1/H1	66	11	−1.68	0	
22	PD	F	71	H1/H1	62	14	0	−0.47	
23	PD	M	72	H1/H1	70	2	1.71	−0.44	
24	PD	M	81	H1/H1	76	6	1.88	0.14	
25	PD	F	44	H1/H1	40	5	−3.56	0.15	
26	PD	F	79	H1/H1	NA	NA	NA	NA	PD 26
27	PD	F	68	H1/H1	55	15	1.65	0	
28	PD	M	57	H1/H1	50	8	NA	NA	PD 28
	ratio F:M/mean ± SD	10:8	70.4 ± 11.2		57.4 ± 11.9	12.5 ± 7.1	0.05 ± 1.5	−0.07 ± 0.18	

MMSE, Mini-Mental State Examination; NA, not available; UPDRS, Unified Parkinson's Disease Rating Scale.
[a]Average rate of decline per year over a minimum of 2 years.

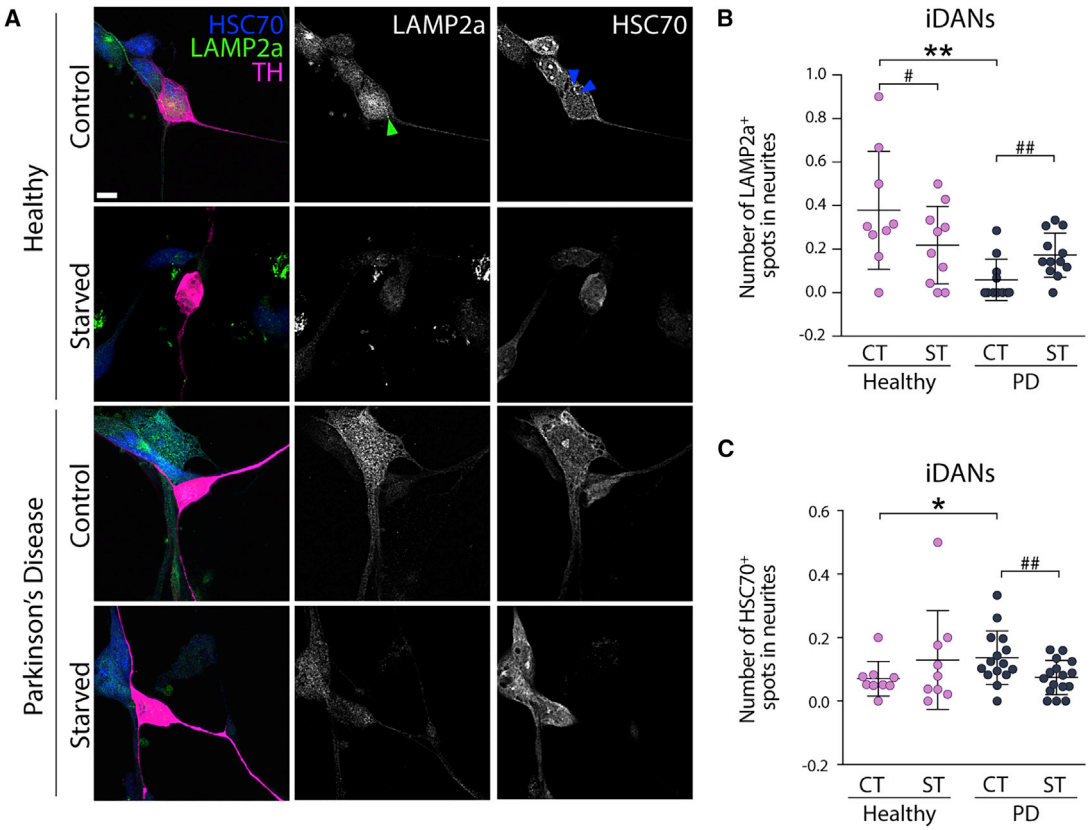

Figure 2. Chaperone-mediated autophagy impairment in PD-iDANs

(A) LAMP2a-positive dot expression and spot detection analysis of LAMP2a-positive (green arrowhead) and HSC70-positive (blue arrowheads) puncta in TH-positive iDANs. Scale bar, 10 μm.

(B) Quantification of LAMP2a-positive puncta in the neurites of TH-positive iDANs (mean average of 14 TH-positive cells assessed per line, n = 10 healthy and n = 18 Parkinson's disease lines). Kruskal-Wallis test, Dunn's multiple comparisons test: *p = 0.0067. Healthy: two-tailed paired t test, $^{\#}$p = 0.0194, df = 8. Parkinson's disease: Wilcoxon matched pairs signed rank test, $^{\#\#}$p = 0.0098, rs = 0.339. Data are expressed as mean ± the SD.

(C) Quantification of HSC70-positive puncta in neurites of TH-positive iDANs (mean average of 95 TH-positive cells assessed per line, n = 8–9 healthy and n = 16 Parkinson's disease lines). Mann-Whitney U test: *p = 0.0128, U = 26.5. Wilcoxon matched pairs signed rank test: $^{\#\#}$p = 0.0031, rs = 0.395. CT, control; H, healthy; PD, Parkinson's disease; ST, starved. Data are expressed as mean ± the SD.

basal rate of CMA in PD-iDANs (Figures 2A and 2B). Importantly, starvation induced a decrease in LAMP2a-positive cytoplasmic puncta in neurites only in H-iDANs, suggesting that PD-iDANs have an altered response to starvation, and that this alteration is specific to the DA subtype (Figures 2A and 2B). We next looked at HSC70 expression, the main chaperone responsible for the degradation of αSYN via CMA (Cuervo and Wong, 2014). Both parental aHDFs from healthy and PD donors showed a decrease in HSC70 expression in response to starvation (Figures S2H and S2I). While the number of HSC70-positive puncta in the neurites of starved H-iDANs increased (154.0% ± 117.2% of the non-starved condition), starvation-induced autophagy led to a decrease of HSC70-positive puncta in PD-iDANs (55.9% ± 28.1% of the non-starved condition) (Figure 2C). At baseline, an increase in the colocalization between HSC70 and αSYN was observed in iDANs from the PD group compared with healthy controls (Figure S2O). However, this was not accompanied by a decrease in αSYN in PD-iDANs following starvation (Figures S2P and S2Q). Taken together, these results suggest that there is both an alteration in baseline CMA as well as stress-induced autophagy that is specific to idiopathic PD-derived iDANs.

Altered macroautophagy response to stress-induced autophagy in iNs from PD patients

CMA preferentially degrades specific proteins, rather than organelles and other macromolecules (Salvador et al., 2000). However, while there is considerable crosstalk between CMA and macroautophagy, starvation predominantly induces macroautophagy, a process involving the formation of double-membraned autophagosomes that

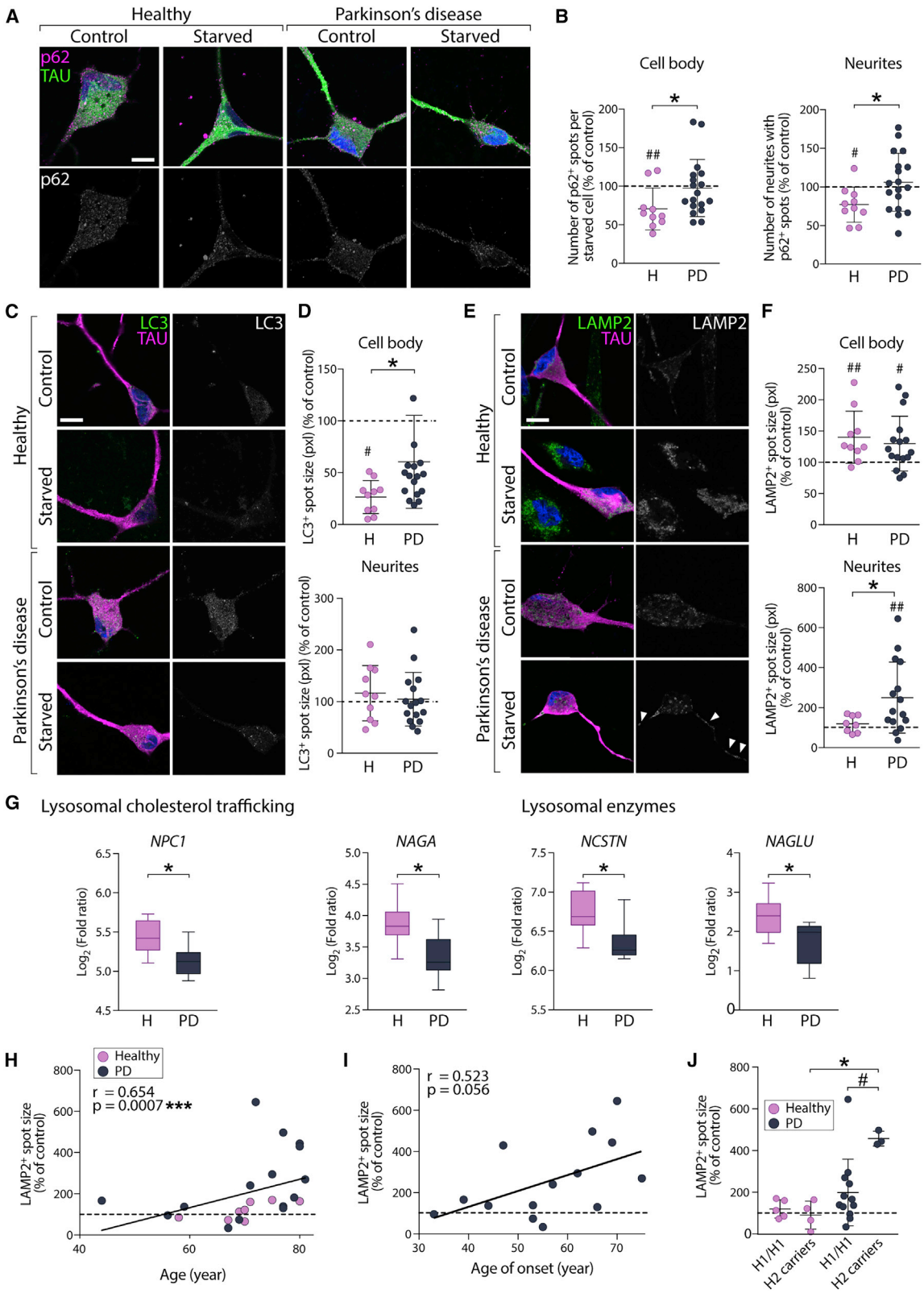

(legend on next page)

fuse with lysosomes, resulting in degradation of their contents. Given that we observed CMA alteration in PD-iDANs in response to starvation, we sought to further investigate whether there is an impairment in macroautophagy in PD-iNs. To validate the activation of macroautophagy upon starvation, we first looked at the cargo receptor p62, which decreases in the context of nutrient deprivation (Pircs et al., 2012). In the parental aHDFs, our starvation regimen induced a decrease in p62-positive cytoplasmic puncta in both healthy and PD donor-derived lines (Figures S3A and S3B). This decrease was also observed in H-iNs (70.6% ± 27.2% of the non-starved condition in the cell body and 77.1% ± 22.8% in neurites) (Figures 3A and 3B). However, once converted to neurons, the majority of PD lines failed to degrade p62 upon starvation, resulting in an accumulation of p62-positive puncta in PD-iNs compared with H-iNs, which was observed in all TAU-positive iNs, regardless of the neuronal subtype or neuronal compartment (97.5% ± 37.1% of the non-starved condition in the cell body and 106.0% ± 37.4% in neurites) (Figures 3A and 3B; see representative images of the puncta quantified in Figures S3G–S3I). We then assessed more specifically microtubule-associated protein 1 light chain 3 beta (LC3) to identify autophagic structures (Pircs et al., 2018). We found that starvation significantly reduced the size of LC3-positive cytoplasmic puncta in the cell bodies of H-iNs (26.5% ± 15.9% of the non-starved condition). However, LC3-positive cytoplasmic puncta in the cell body of PD-iNs were not significantly smaller after starvation (56.5% ± 44.2% of the non-starved condition). When comparing the level of size reduction of LC3-positive cytoplasmic puncta in the cell body after starvation, PD-iNs failed to reduce puncta size to the level that was seen in the H-iN group (Figures 3C and 3D), whereas no effect of starvation was observed in the neurites of H-iNs and PD-iNs (116.3% ± 53.6% of the non-starved condition for H-iNs, and 104.4% ± 51.8% for PD-iNs). Furthermore, this difference in macroautophagy between H-iNs and PD-iNs in the cell bodies was a cell-type-specific feature as it was not seen in the parental aHDFs (Figures S3C and S3D).

Once autophagosomes have enclosed their autophagy substrates, they can fuse with endosomes or lysosomes to form amphisomes and autolysosomes. We thus used LAMP2 (detecting all three isoforms: LAMP2a, LAMP2b, and LAMP2c) to visualize these structures. LAMP2-positive cytoplasmic puncta decreased upon starvation in the parental aHDFs of PD lines (Figures S3E and S3F). However, while an increase of the size of these structures upon starvation was similar in the cell bodies of both H- and PD-iNs (140.1% ± 41.6% of the non-starved condition for H-iNs and 130.06% ± 43.8% for PD-iNs), in the neurites, the size of LAMP2-positive puncta was unaffected by starvation in H-iNs (118.9% ± 42.3% of the non-starved condition), whereas they were significantly bigger in PD-iNs (251.8% ± 177.7% of the non-starved condition) (Figures 3E and 3F). Unlike the altered CMA

Figure 3. Accumulation of p62, LC3, and LAMP2 in PD-iNs upon starvation

(A) p62-positive dot expression in TAU-positive iNs. Scale bar, 10 μm.

(B) Quantification of p62-positive puncta in TAU-positive iNs (mean average of 577 TAU-positive cells assessed per line, n = 10 healthy and n = 18 Parkinson's disease lines). Cell body: Mann-Whitney test, *p = 0.0400; healthy, two-tailed paired t test, $^{\#\#}$p = 0.0056, df = 9. Neurite: unpaired t test, *p = 0.0357, df = 26, healthy, two-tailed paired t test, $^{\#}$p = 0.0128, df = 9. Data were normalized as percentage of control condition (not starved) and are expressed as mean ± the SD.

(C) LC3-positive dot expression in TAU-positive iNs. Scale bar, 10 μm.

(D) Quantification of LC3-positive puncta in TAU-positive iNs (mean average of 479 TAU-positive cells assessed per line, n = 10 healthy and n = 18 Parkinson's disease lines). Cell body: two-tailed Mann-Whitney U test, *p = 0.0311, U = 51; healthy, two-tailed paired t test, $^{\#\#}$p = 0.0051, df = 9. Data were normalized as percentage of control condition (not starved) and are expressed as mean ± the SD.

(E) LAMP2-positive dot expression in TAU-positive iNs. Scale bar, 10 μm.

(F) Quantification of LAMP2-positive puncta in TAU-positive iNs (mean average of 202 TAU-positive cells assessed per line, n = 10 healthy and n = 17 Parkinson's disease lines). Cell body: healthy, two-tailed paired t test, $^{\#\#}$p = 0.0078, df = 8; Parkinson's disease, $^{\#}$p = 0.0295, df = 13. Neurites: two-tailed unpaired t test with Welch's correction, *p = 0.0136, U = 24; *p = 0.0125, df = 18.23. Parkinson's disease: two-tailed paired t test, $^{\#\#}$p = 0.0042, df = 16.75. Data were normalized as percentage of control condition (not starved) and are expressed as mean ± the SD.

(G) Boxplots of $\log_2$ fold changes in expression of genes associated with lysosomal functions (adjusted p value <0.09, n = 10 healthy and n = 10 Parkinson's disease lines). Data are expressed as mean ± the SD.

(H) Accumulation of LAMP2-positive puncta upon stress-induced autophagy is associated with the age of the donor (n = 23 lines). Spearman's rank correlation: ***p = 0.0007; 95% confidence interval, 0.3199–0.8437.

(I) Association between accumulation of LAMP2-positive puncta upon stress-induced autophagy and the age of onset of Parkinson's disease (n = 14 Parkinson's disease lines). Spearman's rank correlation: p = 0.056; 95% confidence interval, 0.01127–0.8263.

(J) More pronounced accumulation of LAMP2-positive puncta upon stress in *MAPT H2* carrier Parkinson's disease patients. Kruskal-Wallis test, Dunn's multiple comparisons test: *p = 0.0265. Two-tailed Mann-Whitney U test: $^{\#}$p = 0.0250, U = 3. Data are expressed as mean ± the SD. CT, control; H, healthy; PD, Parkinson's disease; ST, starved.

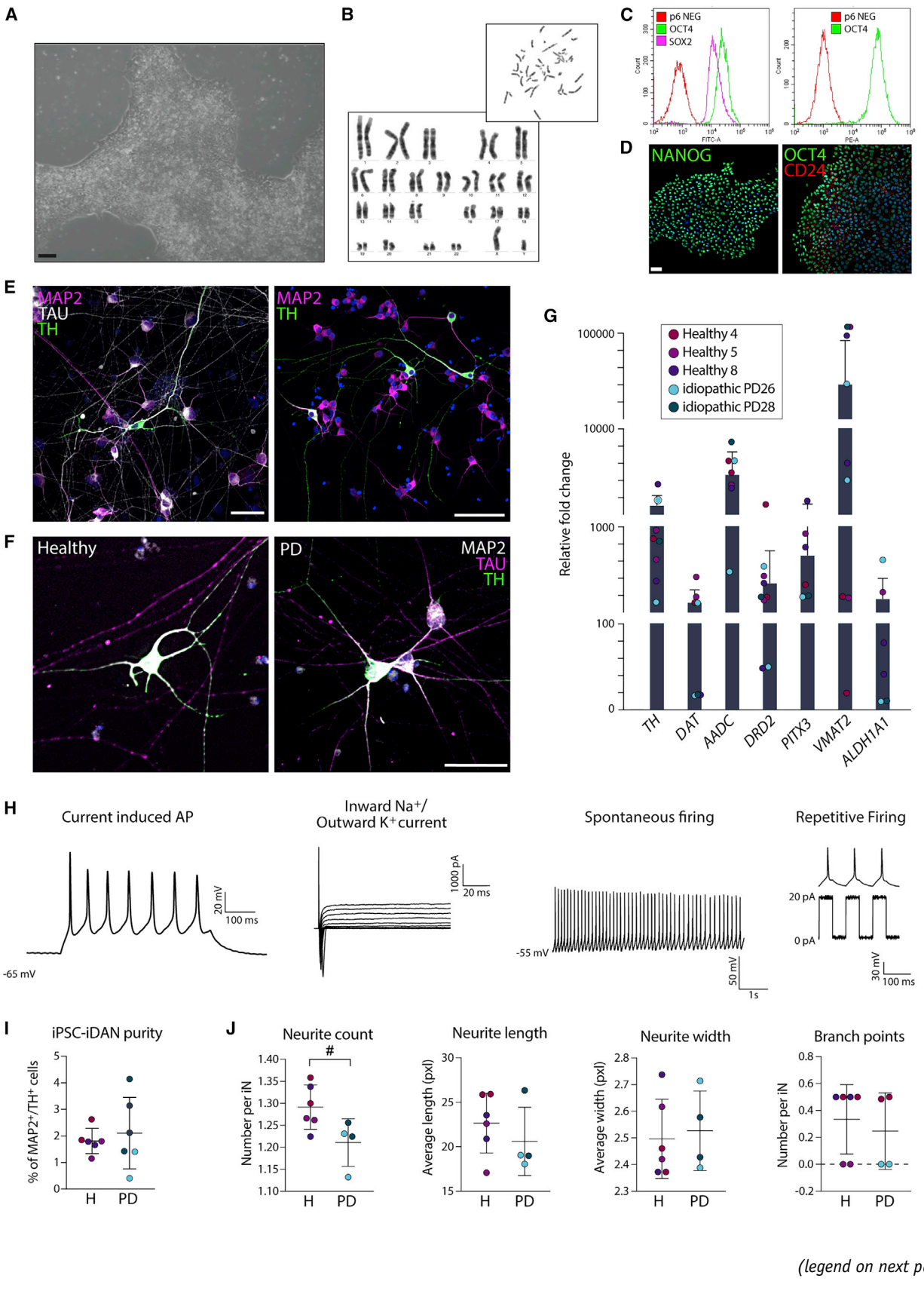

(legend on next page)

response (Figures 2A–2C), these phenotypes were present in all iNs and not just DA neurons (Figure S4). Blocking the autophagic flux using bafilomycin A1 led to an accumulation of LC3-positive puncta in the cell body of H-iNs. However, this accumulation of autophagosomes was absent in PD-iNs (Figures S6C–S6E), indicating possible impairment at early steps of the autophagic process, as also supported by a downregulation of early autophagy-related genes in PD-iNs (Figure S6F).

To assess whether this altered autophagy response could be due to basal changes in the transcriptome of PD-iNs, we performed RNA sequencing (RNA-seq) analysis on the iNs and the parental aHDFs. This analysis confirmed there was a major change in gene expression profile as aHDFs were reprogrammed toward a neuronal phenotype (Figure S5). Moreover, gene set enrichment analysis (GSEA) using Kyoto Encyclopedia of Genes and Genomes (KEGG) pathways identified genes in the lysosome pathway (hsa014142) to be significantly enriched (adjusted p value = 0.026) (Figure S6A). When analyzing specifically the lysosomal genes, we found that the lysosomal cholesterol trafficking gene *NPC1* involved in the inherited metabolic disease Niemann-Pick, type C (Park et al., 2003) as well as three other lysosomal enzymes (*NAGA*, *NCSTN*, *NAGLU*) were downregulated in PD-iNs compared to H-iNs (Figure 3G), supporting the data suggesting that there are alterations in lysosomal functions at baseline and in line with observations that these inherited disorders can lead to parkinsonian states clinically and pathologically (Winder-Rhodes et al., 2012). Importantly, when analyzing expression of these genes between the healthy controls and PD patients in parental aHDFs, they were not differentially expressed (Figure S6B).

Age-related correlation in disease-associated impairments and accumulation of phosphorylated αSYN

Recent reports have shown that age-associated properties of the human donors are maintained in iNs but not in iPSC-derived neurons (Capano et al., 2022; Huh et al., 2016; Kim et al., 2018; Mertens et al., 2015, 2021; Tang et al., 2017). We therefore assessed whether the accumulation of lysosomal structures in H- and PD-iNs was associated with the age of the donor. We found a positive correlation between the age and the accumulation of lysosomes in neurites (Figure 3H), and a trend toward a positive correlation of this accumulation with age of onset at diagnosis (Figure 3I). This was more pronounced in lines derived from patients carrying the H2 haplotype of *MAPT*, which has previously been associated with a more rapid progression and cognitive decline in PD and other neurodegenerative disorders (Figure 3J) (Valenca et al., 2016; Vuono et al., 2015).

To further study donor age and how this affects disease-related pathology, we next established iPSC lines from the aHDFs of two patients (with a high amount of pathology as quantified in the iNs derived from same patient's aHDFs) and three controls (see Table 1). The cells were reprogrammed into iPSCs using the StemRNA 3rd Generation Reprogramming Kit (Figure 4A). Quality control analysis confirmed that the iPSCs retained a normal karyotype (Figure 4B), and expression of pluripotency markers was confirmed using immunocytochemistry and flow analysis (Figures 4C and 4D). We then confirmed that the same protocol developed for the fibroblast-to-iDAN conversion (Figure 1A) also converted iPSCs to functional iDANs (Figures 4E and 4F). iPSC-iDANs expressed high levels of DA-related genes (Figure 4G) and were functionally mature (Figure 4H). Similarly to fibroblast-derived iDANs, there was no difference in neuronal purity, although a slightly lower neurite count was observed in iPSC-derived iDANs from PD patients (Figures 4I and 4J).

Next, we used RNA-seq from iNs derived from aHDFs (Fib-iNs) and iNs derived from iPSCs (iPSC-iNs) from the same individuals to assess age-related aspects in the resulting neurons (Figure 5A). First, GSEA was performed to determine if any molecular features relating to cellular

Figure 4. Generation of iDANs from iPSCs of healthy donors and idiopathic PD patients

(A) Brightfield images of fibroblasts reprogrammed to iPSCs using a StemRNA 3rd Generation Reprogramming Kit. Scale bar, 100 μm.
(B) Cells retained a normal karyotype.
(C) FACS quantification of stem cell markers OCT4, SOX2, and CD24.
(D) Immunofluorescence staining showing that cells express stem cell markers NANOG, OCT4, and CD24. Scale bar, 50 μm.
(E) MAP2-positive, TAU-positive, and TH-positive iPSC-iDANs. Cells are counterstained with DAPI (in blue). Scale bars, 100 μm.
(F) Representative images of MAP2-positive, TAU-positive, and TH-positive iPSC-iDANs derived from healthy donors and PD patients. Cells are counterstained with DAPI (in blue). Scale bars, 25 μm.
(G) Quantitative RT-PCR gene expression quantification of DA genes relative to parental iPSC levels (nine clones from five lines). Refer to Table 1 for information on each donor from which the iPSC cell lines were derived. Data are expressed as mean ± the SD.
(H) Patch clamp recordings of iDANs reprogrammed from RC17 embryonic stem cells at day 35 (n = 8 neurons).
(I) Quantification of double-MAP2-positive and TH-positive cells (from two clones; six well replicates). Data are expressed as mean ± the SD.
(J) Quantification of neurite profile in TAU-positive H-iNs and PD-iNs derived from iPSCs (from two clones; six well replicates). Data are expressed as mean ± the SD.

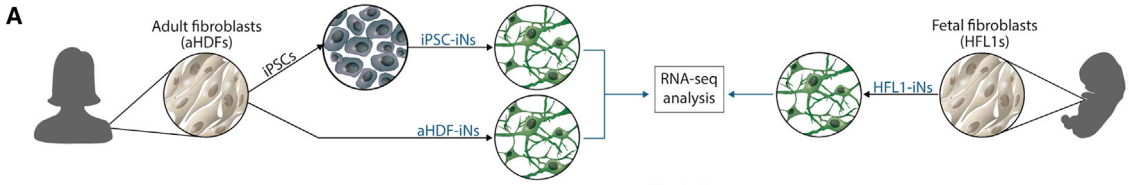

B

Description	Set size	Enrichment Score	NES	*p* value	*p*-adjust
GO_MULTICELLULAR_ORGANISM_AGING	28	-0.627	-1.872	0.003	0.015
GO_AGING	265	0.296	1.120	0.217	0.460
GO_NEGATIVE_REGULATION_OF_CELL_AGING	21	-0.432	-1.201	0.230	0.460
GO_REGULATION_OF_CELL_AGING	42	-0.320	-1.015	0.425	0.594
GO_POSITIVE_REGULATION_OF_CELL_AGING	12	-0.372	-0.887	0.581	0.594
GO_CELL_AGING	96	-0.249	-0.935	0.594	0.594

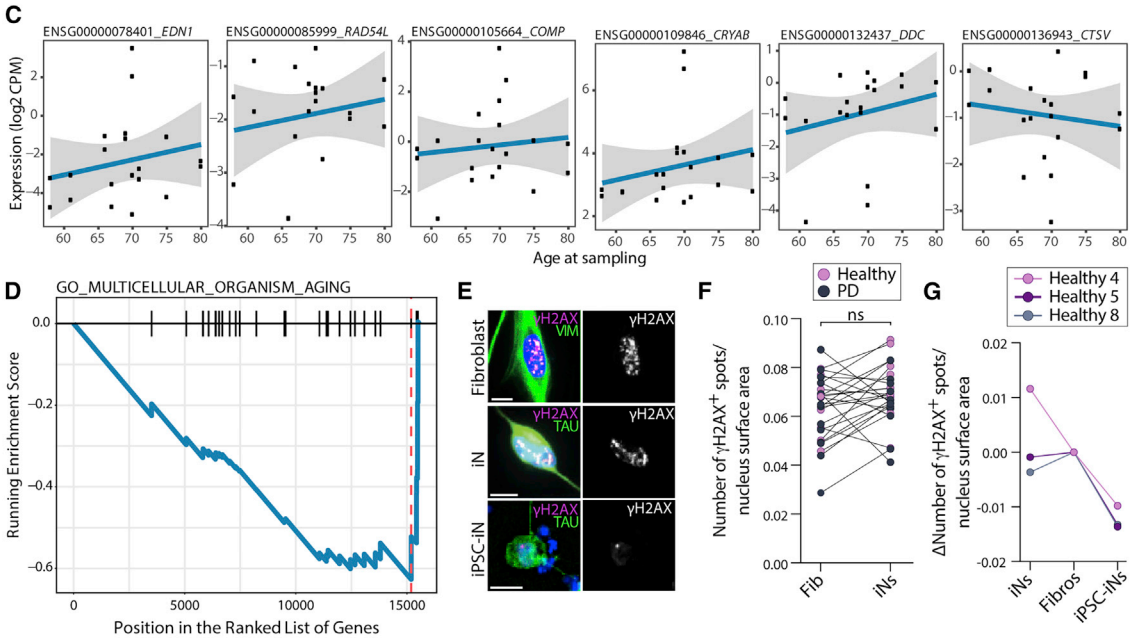

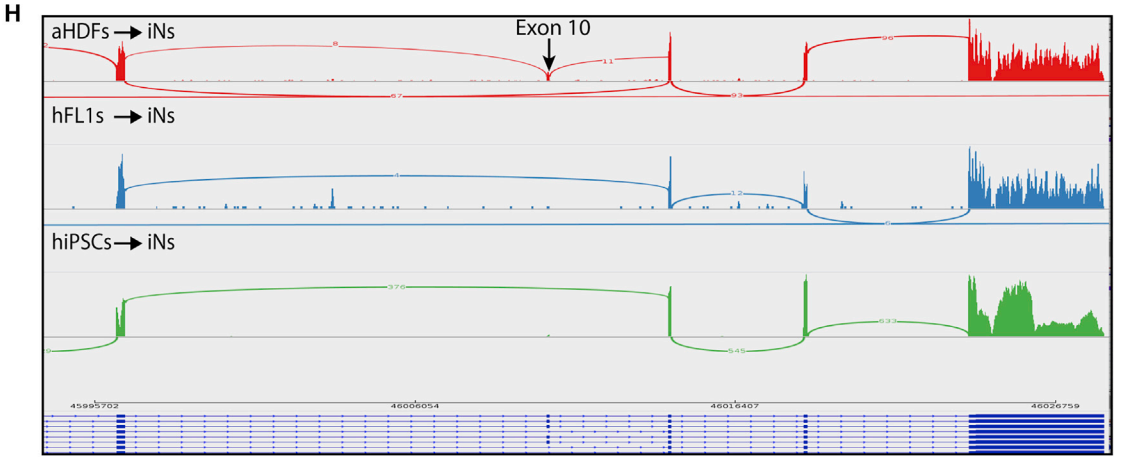

(legend on next page)

aging were associated with the donor age in Fib-iNs. Genes were ranked based on their association (using the Pearson correlation coefficient) with age at sampling and six gene sets related to aging were extracted from the Gene Ontology database. Despite the limited age span of the donors included in this analysis (58–80 years old), we observed a positive correlation between donor age with expression of an age-related gene signature (normalized enrichment score 1.4, adjusted p value = 0.015) in Fib-iNs (adjusted p value = 0.4; Figures 5B–5D). To complement the GSEA data, we also looked at DNA damage, another independent marker of cellular aging, using γH2AX. This analysis comparing the number of γH2AX spots in the nucleus of parental aHDFs with reprogrammed iNs showed a maintenance of the number of γH2AX spots after 27 days of conversion, which was not the case following reprograming of these same cell lines to iPSC-iNs, indicating a rejuvenation of the cells during reprograming to pluripotency (Figures 5E–5G). Next, we looked at the presence of the isoforms of TAU expressed in adult mature neurons. There are three TAU isoforms with three repeats (3R) and three with four repeats (4R). Neurons generated from iPSCs very strongly express the 3R isoforms but do not express the 4Rs at the protein level, even after 1 year of *in vitro* maturation (Sposito et al., 2015), reflecting the expression of only the 3Rs of TAU at the human embryonic stage. This analysis showed that exon 10 (giving rise to 4R isoforms) is only expressed in iNs from aHDFs (in ∼40% of transcripts), and not in iNs derived from fetal fibroblasts or from iPSCs (Figure 5H). Moreover, the 3R/4R ratio for aHDFs was 23%, whereas it was <1% for hFL1s. Taken together, this analysis suggests that donor age is at least partially maintained during iN conversion but erased during iPSC reprogramming, similar to other reports (Capano et al., 2022; Mertens et al., 2015; Tang et al., 2017).

Phosphorylated αSYN is a hallmark of PD pathology and this has been recapitulated in some iPSC-based cellular models of genetic forms of PD (Kouroupi et al., 2017; Lin et al., 2016) but not idiopathic PD. We therefore sought to investigate whether alterations in stress-induced autophagy observed in Fib-iNs from idiopathic PD patients could lead to changes in the levels of phosphorylated αSYN at the serine 129 site (pSer129 αSYN). We found that while a concurrent activation of macroautophagy by starvation and a blockage of the flux with bafilomycin A1 did not induce significant changes in pSer129 αSYN in H-iNs (83.1% ± 53.9% of the starved condition), it did lead to an increase in the number of PD-iNs with pSer129 αSYN-positive cytoplasmic dots (126.5% ± 54.0% of the starved condition) (Figures 6A and 6B). This increase was also observed when looking specifically at PD-iDANs (128.1% ± 21.4% of the starved condition), compared with H-iDANs, which again did not show any changes in pSer129 αSYN upon bafilomycin A1 treatment (98.2% ± 16.0% of the starved condition) (Figures 6D and 6E). Positive correlation between the accumulation of 81A-positive puncta in two independent experiments evaluating the pSer129 αSYN spot expression in iNs and in iDANs showed that the same cell lines are prone to pSer129 αSYN accumulation independently of the neuronal subtype, and demonstrates the reproducibility of these experiments (Figure S6G). Interestingly, for some of the results including pSer129 αSYN, p62, and LAMP2 accumulation, subanalyses allowed a stratification of the PD patient population based on their age and age at onset (Figures S3J and S6I). Finally, to assess whether elevated basal levels of total αSYN could explain the elevated levels of pSer129 αSYN observed in lines starved and treated with bafilomycin A1, we plotted the measure of the total αSYN fluorescence intensity against the pSer129 αSYN expression

Figure 5. Assessment of cellular aging

(A) Overview of RNA-seq experiment.

(B) Gene set enrichment analysis (GSEA) showing enrichment scores of pathways related to cell aging.

(C) Top genes showing a clear increase in expression with age were extracted from the Gene Ontology database and queried against using GSEA (as implemented in the clusterProfiler R package). Five out of six of these gene sets showed negative enrichment scores, indicating association of aging with donor age in this dataset.

(D) Multicellular organism aging showing a significant enrichment score.

(E) Representative image of γH2AX expression in TAU-positive iNs, parental fibroblasts and iPSC-iNs, all from line #18 (87 years old). Scale bar, 10 μm.

(F) Quantification of γH2AX-positive puncta in TAU-positive iNs and parental fibroblasts (mean average of 1,327 fibroblasts and 1,210 TAU-positive cells assessed per line, n = 26 lines). Two-tailed paired t test: p = 0.071, df = 25.

(G) Quantification of γH2AX-positive puncta in TAU-positive iNs, parental fibroblasts and iPSC-iNs (mean average of n = 329 fibroblasts, n = 833 TAU-positive iNs, and n = 24 iPSC-iNs assessed per line, n = 3 lines). Refer to Table 1 for the information of each donor from which the iPSC cell lines were derived.

(H) Sashimi plots visualizing splice junctions and genomic coordinates from merged bam files from adult Fib-iNs (red) and fetal Fib-iNs (blue) indicating that expression of exon 10 (4R isoforms) is only present in iNs from adult fibroblasts. Height of bars indicates expression level and the number on the lines gives number of reads spanning that splice junction. ns, not significant; Vim, vimentin.

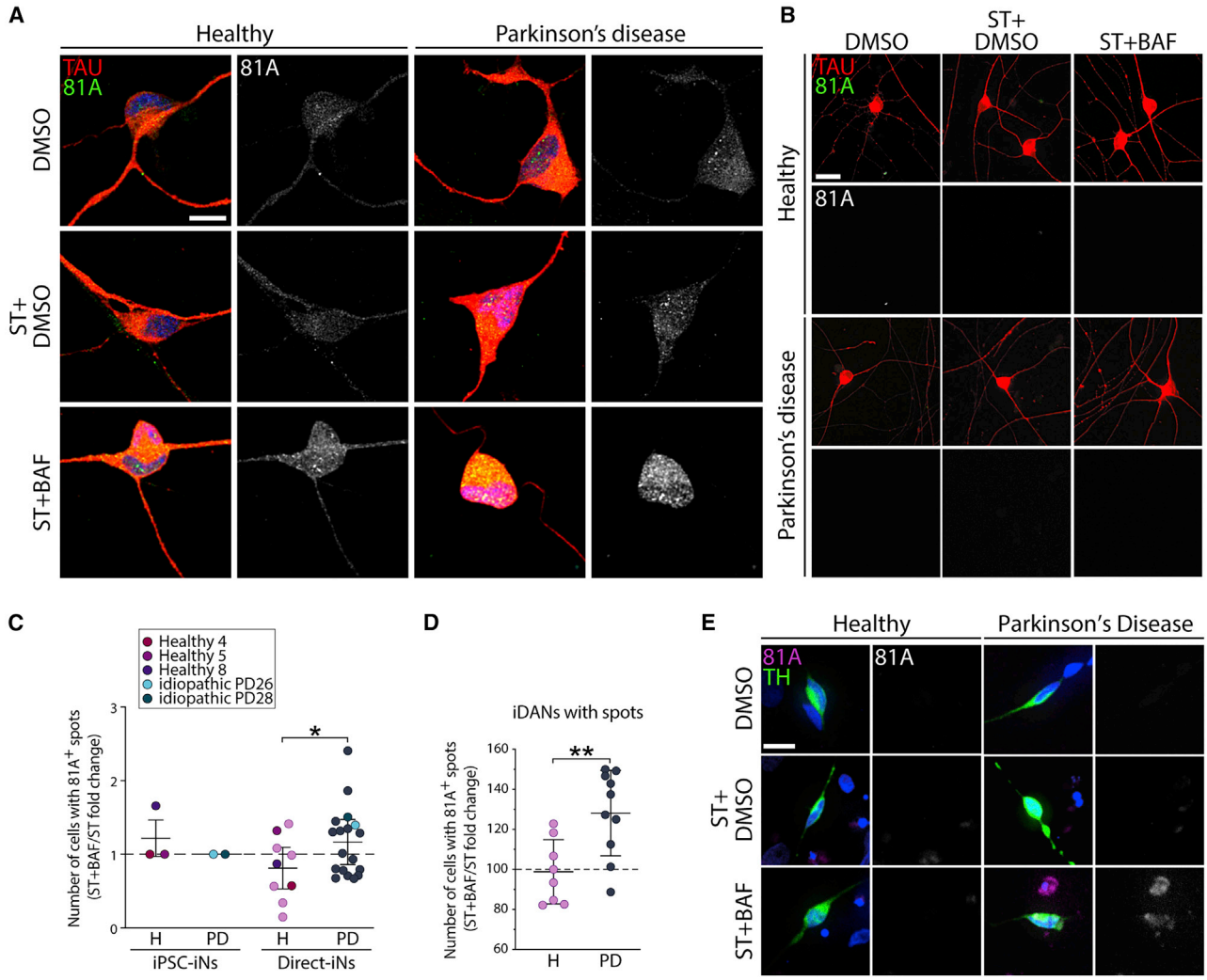

Figure 6. Autophagy impairments lead to an accumulation of phosphorylated αSYN in PD-iNs and PD-iDANs

(A) Confocal images of 81A-positive dot expression in TAU-positive iNs directly reprogrammed from fibroblasts. Scale bar, 10 μm.

(B) Fluorescent images of 81A-positive dot expression in TAU-positive iNs reprogrammed from iPSCs. Scale bar, 25 μm.

(C) Quantification of TAU-positive iNs with 81A-positive (pSer129 αSYN) puncta in the cell body (iPSCs-iNs: mean average of 180 TAU-positive cells assessed per line, n = 3 healthy and n = 2 PD lines. Direct-iNs: mean average of 1,461 TAU-positive cells assessed per line, n = 9 healthy and n = 18 PD lines). Two-tailed unpaired t test: *p = 0.0329, df = 25. Refer to Table 1 for the information of each donor from which the iPSC cell lines were derived. Data are expressed as mean ± the SD.

(D) Quantification of TAU-positive/TH-positive iDANs with 81A-positive puncta in the cell body (mean average of 28 TAU-positive/TH-positive cells assessed per line, n = 8 healthy and n = 10 PD lines). Two-tailed unpaired t test: **p = 0.0054, df = 16. Data are expressed as mean ± the SD.

(E) 81A-positive dot expression (in magenta) in TH-positive iDANs (in green) directly reprogrammed from fibroblasts. Scale bar, 25 μm.

BAF, bafilomycin A1; H: healthy; PD, Parkinson's disease; ST, starved.

measured in iDANs. There was no correlation between basal total αSYN levels and the bafilomycin A1-induced accumulation of pSer129 αSYN in iDANs (Figure S6H), suggesting that the increase seen in the PD group is not due to higher basal αSYN expression (Figures S2L–S2N). When assessing iN reprogrammed from iPSCs established from the two PD lines showing the most pSer129 αSYN accumulation in fibroblast-derived iNs and iDANs as well as three control lines (Table 1), we could not detect any pSer129 αSYN puncta in the resulting iPSC-iNs in these lines (Figures 6B and 6C), supporting that the maintenance of age in iNs is important for modeling the αSYN pathophysiology of idiopathic PD.

DISCUSSION

We report on an improved cellular model of idiopathic PD using a *REST* knockdown approach to enable neuronal gene transcription in aHDFs (Drouin-Ouellet et al., 2017), combined with an optimal combination of DA fate determinants (*Lmx1a*, *Lmx1b*, *Foxa2*, *Otx2*, *Nr4a2*). This new direct reprogramming approach increased the efficiency, subtype identity, and functional maturation of iDANs during direct conversion, making it possible to perform studies at a scale suitable for disease modeling, drug screening, and other biomedical applications. The model is much less labor intensive and cost-effective than iPSC-modeling, which allowed us to compare iNs from 18 different idiopathic PD patients that were all processed at the same time. Moreover, it maintains the donor's age and reflect pathological changes after only 25 days.

We observed alterations in stress-induced autophagy across the different patient-derived iNs compared with healthy donor lines. We found that blocking the autophagic flux through the inhibition of the fusion of autophagosomes with lysosomes resulted in accumulation of pSer129 αSYN in PD-iNs and PD-iDANs. These impairments of autophagy-lysosomal function may reflect the effect of the important presence of variants of genes related to lysosomal storage disorders in the PD patient population. Indeed, a recent study reported that more than half of the cases in a PD patient cohort harbored one or more putative damaging variants among the lysosomal storage disorders genes, suggesting the possibility that these variants may interact in a multi-hit, combinatorial manner to degrade lysosomal function, causing the accumulation of αSYN and increasing susceptibility to PD (Robak et al., 2017). Future studies using lines derived from patients with strong genetic forms of PD will also help our understanding of the phenotypes found in the idiopathic PD lines and how they relate to different pathways disrupted in familial PD.

Disease-associated impairment could not be detected in the parental aHDFs, nor in the same cells when they were first reprogrammed to pluripotency and then converted to DA neurons. This shows that direct conversion of aHDFs, where age-related aspects of the donor are maintained, provides a faithful cell-based model of idiopathic PD. Importantly, our cellular model showed that iNs from different patients are not impaired to the same degree. We found that the degree of impairment relates, at least to some extent, to the age of the donor, the age at PD onset, and the *MAPT* haplotype. This effect of age and genetic variance on disease pathology has not been recapitulated in cellular models before, and suggests that direct conversion to iDANs could be used for differential diagnostics, drug screening, and disease modeling of late-onset neurogenerative diseases while also capturing the heterogeneity of disease that is apparent clinically.

In this respect, our results demonstrate the utility of establishing models of neurodegenerative disorders with cells that resemble the subtype and functionality of the affected neurons in individual patients as closely as possible. For example, we could not detect any autophagy-related impairment in the aHDFs prior to conversion, clearly demonstrating that the reprogramming to neurons is essential to reveal disease-related phenotypes. Also, specific CMA impairments were detected only in iNs with a DA phenotype.

While it is hard to draw exact parallels between stem-cell derived neurons formed via developmental principles and directly converted neurons, both systems have their own merits. Of importance here is that the aging signature of the donor cell is maintained during direct conversion when postmitotic neurons are formed without a proliferative intermediate. Our data support the maintenance of donor age, which uniquely allows for modeling age-related aspects of PD. Future studies using this cellular model will thus contribute to a deeper understanding of the age-associated pathology of PD along with the cellular basis of disease subtypes and variable progression and, by so doing, allow us to better develop and assess novel therapeutic interventions.

EXPERIMENTAL PROCEDURES

Cell lines

aHDFs were obtained from the Parkinson's Disease Research Clinic at the John van Geest Centre for Brain Repair (Cambridge, UK) and used under full local ethical approvals: REC 09/H0311/88 (University of Cambridge) and CERSES-18-004-D (University of Montreal) (Table 1). The subjects' consent was obtained according to the declaration of Helsinki. Cell lines used in this study will be made available to others subject to appropriate ethical approval and an MTA from the requestor. For biopsy sampling information see Drouin-Ouellet et al. (2017).

Neural reprogramming

For direct neural reprogramming, aHDFs were plated at a density of 26,300 cells/cm^2 in 24-well plates (Nunc) according to a previously published protocol (Shrigley et al., 2018). Prior to plating, the wells were coated overnight with either 0.1% gelatin (Sigma), or a combination of polyornithine (15 μg/mL), fibronectin (0.5 ng/μL), and laminin (5 μg/mL). To assess the reprogramming efficiency of each line, all 28 lines were reprogrammed at the same time with the same virus mixture, and this was repeated three times using different batches of virus for each of the eight lentiviral vectors required for the iDAN reprogramming.

Starvation and bafilomycin A1 treatment

On day 28 following viral transduction, iNs were starved for 4 h by replacing the culture medium with HBSS and Ca^{2+}/Mg^{2+} and

compared with the condition without starvation, where cells were left in their original culture medium. The duration of starvation treatment was chosen based on a starvation curve performed on the iNs (0, 2, and 4 h), which showed clear increases in p62 and LC3 expression by WB in the absence of neuronal cell death (Figures S2D and S2E). For the experiment with bafilomycin A1, cells were starved in HBSS Ca^{2+}/Mg^{2+} containing bafilomycin A1 (100 nM; Sigma Aldrich) for 2 h and compared with cells incubated in HBSS Ca^{2+}/Mg^{2+} containing dimethyl sulfoxide (DMSO; vehicle). This regimen was chosen based on the increase of LC3-II and the LC3-II/LC3-I ratio as assessed by WB. At the end of the incubation period, cells were fixed in 4% paraformaldehyde.

High-content screening quantifications

The total number of DAPI-positive, TAU-positive, and TH-positive cells per well, as well as the average fluorescence intensity for αSYN, was quantified using the Cellomics Array Scan (Array Scan VTI, Thermo Fisher). Average dot number and size were measured in those neurons in which the cytoplasm and neurites were defined by TAU or TH staining. Puncta of p62, LC3, LAMP2, LAMP2a, HSC70, αSYN, and 81A were detected (using a spot-detection program) and measured in each case. Images with cells with extreme values were manually verified to make sure that poor focus was not underlying these results. The primary antibodies used are listed in Table S1. Cell images in Figures 2, 3A, 3C, 3E, 6A, 6B, and 6E are representatives images acquired by confocal microscopy (Zeiss LSM800) at 63×.

Statistical analysis

All data are expressed as mean ± the SD. Whenever the analysis is performed with one cell line, three to four well replicates were used. In case of experiments using multiple cell lines, we used a minimum of n = 6 to account for inter-individual variation. A Shapiro-Wilk normality test was used to assess the normality of the distribution. When a normal distribution could not be assumed, a non-parametric test was performed. Groups were compared using a one-way ANOVA with a Bonferroni post hoc or a Kruskal-Wallis test with a Dunn's multiple comparisons tests. To determine whether there was a significant difference between two sets of observations repeated on the same lines, a paired sample t test was also performed. In cases of only two groups, they were compared using a Student's t test. An F test was used to compare variance and, in cases of unequal variance, a Welch's correction test was then performed. Statistical analyses were conducted using the GraphPad Prism 7.0. An alpha level of $p < 0.05$ was set for significance.

See supplemental experimental procedures for further details.

Data and code availability

The accession number for the RNA-seq dataset reported in this paper is GEO: GSE125239.

SUPPLEMENTAL INFORMATION

Supplemental information can be found online at https://doi.org/10.1016/j.stemcr.2022.08.010.

AUTHOR CONTRIBUTIONS

J.D.-O., K.P., J.J., R.A.B., and M. Parmar designed the research. J.D.-O., E.M.L., F.N., K.P., J.B., F.P., M.B., S.S., M. Pereira, A.B., M.K., R.V., T.B.S., and K.P. performed the research. D.R.O., A.F., and R.A.B. contributed new reagents/analytic tools. J.D.-O., E.M.L., F.N., K.P., J.B., F.P., M.B., S.S., P.S., Y.S., R.V., and K.P. analyzed data. J.D.-O. and M. Parmar wrote the first draft of the paper.

ACKNOWLEDGMENTS

We thank Marie Persson Vejgården, Sol Da Rocha Baez, Ulla Jarl (Lund University), as well as Dr. Anna Hammarberg at the MultiPark Cellomics platform at Lund University and Simon-Pierre Gravel (U. Montreal) for their valuable help with high content imaging. This research has received funding from the NYSCF, the ERC FP/2007–2013 NeuroStemcellRepair (no. 602278 and ERC no. 771427), the Swedish Research Council (2016-00873), Parkinsonfonden, Hjärnfonden (FO2019-0301), Olle Engkvist Foundation 203-0006 (J.J.), the Strategic Research Areas at Lund University MultiPark and StemTherapy, the Cure Parkinson's Trust in the UK (RAB), and Parkinson Canada (2018-00236) (J.D.-O.). This research was also supported by the Canada Research Chair Program and the NIHR Cambridge Biomedical Research Centre (BRC-1215-20014). The views expressed are those of the authors and not necessarily those of the NIHR or the Department of Health and Social Care. This research was funded in part by the Wellcome Trust 203151/Z/16/Z. For the purpose of open access, the author has applied a CC BY public copyright license to any author-accepted manuscript version arising from this submission. R.A.B. was a NIHR Senior Investigator. M. Parmar is an NYSCF - Robertson Investigator. J.D.-O. is a Canada Research Chair and received support from FRQS in partnership with Parkinson Québec (#268980) and the Canada Foundation for Innovation (#38354). M.B. and S.S. were funded by the European Union Horizon 2020 Programme (H2020-MSCA-ITN-2015; no. 676408). E.M.L. is supported by an FRQS Graduate Scholarship in partnership with Parkinson Canada.

CONFLICTS OF INTERESTS

M. Parmar, J.J., and J.D.-O. are co-inventors of the patent application PCT/EP2018/062261 owned by New York Stem Cell Foundation. M. Parmar is the owner of Parmar Cells AB.

Received: August 24, 2021
Revised: August 25, 2022
Accepted: August 25, 2022
Published: September 22, 2022

REFERENCES

Ambasudhan, R., Talantova, M., Coleman, R., Yuan, X., Zhu, S., Lipton, S.A., and Ding, S. (2011). Direct reprogramming of adult human fibroblasts to functional neurons under defined conditions. Cell Stem Cell *9*, 113–118.

Brazdis, R.M., Alecu, J.E., Marsch, D., Dahms, A., Simmnacher, K., Lörentz, S., Brendler, A., Schneider, Y., Marxreiter, F., Roybon, L., et al. (2020). Demonstration of brain region-specific neuronal

vulnerability in human iPSC-based model of familial Parkinson's disease. Hum. Mol. Genet. *29*, 1180–1191.

Caiazzo, M., Dell'Anno, M.T., Dvoretskova, E., Lazarevic, D., Taverna, S., Leo, D., Sotnikova, T.D., Menegon, A., Roncaglia, P., Colciago, G., et al. (2011). Direct generation of functional dopaminergic neurons from mouse and human fibroblasts. Nature *476*, 224–227.

Capano, L.S., Sato, C., Ficulle, E., Yu, A., Horie, K., Kwon, J.S., Burbach, K.F., Barthélemy, N.R., Fox, S.G., Karch, C.M., et al. (2022). Recapitulation of endogenous 4R tau expression and formation of insoluble tau in directly reprogrammed human neurons. Cell Stem Cell *29*, 918–932.e8.

Cuervo, A.M., Stefanis, L., Fredenburg, R., Lansbury, P.T., and Sulzer, D. (2004). Impaired degradation of mutant alpha-synuclein by chaperone-mediated autophagy. Science *305*, 1292–1295.

Cuervo, A.M., and Wong, E. (2014). Chaperone-mediated autophagy: roles in disease and aging. Cell Res. *24*, 92–104.

Drouin-Ouellet, J., Lau, S., Brattås, P.L., Rylander Ottosson, D., Pircs, K., Grassi, D.A., Collins, L.M., Vuono, R., Andersson Sjöland, A., Westergren-Thorsson, G., et al. (2017). REST suppression mediates neural conversion of adult human fibroblasts via microRNA-dependent and -independent pathways. EMBO Mol. Med. *9*, 1117–1131.

Huh, C.J., Zhang, B., Victor, M.B., Dahiya, S., Batista, L.F., Horvath, S., and Yoo, A.S. (2016). Maintenance of age in human neurons generated by microRNA-based neuronal conversion of fibroblasts. Elife 5, e18648.

Jiang, H., Xu, Z., Zhong, P., Ren, Y., Liang, G., Schilling, H.A., Hu, Z., Zhang, Y., Wang, X., Chen, S., et al. (2015). Cell cycle and p53 gate the direct conversion of human fibroblasts to dopaminergic neurons. Nat. Commun. *6*, 10100.

Kim, Y., Zheng, X., Ansari, Z., Bunnell, M.C., Herdy, J.R., Traxler, L., Lee, H., Paquola, A.C.M., Blithikioti, C., Ku, M., et al. (2018). Mitochondrial aging defects emerge in directly reprogrammed human neurons due to their metabolic profile. Cell Rep. *23*, 2550–2558.

Kirkeby, A., Nolbrant, S., Tiklova, K., Heuer, A., Kee, N., Cardoso, T., Ottosson, D.R., Lelos, M.J., Rifes, P., Dunnett, S.B., et al. (2017). Predictive markers guide differentiation to improve graft outcome in clinical translation of hESC-based therapy for Parkinson's disease. Cell Stem Cell *20*, 135–148.

Klionsky, D.J., Abdelmohsen, K., Abe, A., Abedin, M.J., Abeliovich, H., Arozena, A.A., Adachi, H., Adams, C.M., Adams, P.D., Adeli, K., et al. (2016). Guidelines for the use and interpretation of assays for monitoring autophagy (3rd edition). Autophagy *12*, 1–222.

Kouroupi, G., Taoufik, E., Vlachos, I.S., Tsioras, K., Antoniou, N., Papastefanaki, F., Chroni-Tzartou, D., Wrasidlo, W., Bohl, D., Stellas, D., et al. (2017). Defective synaptic connectivity and axonal neuropathology in a human iPSC-based model of familial Parkinson's disease. Proc. Natl. Acad. Sci. USA *114*, E3679–E3688.

Lang, C., Campbell, K.R., Ryan, B.J., Carling, P., Attar, M., Vowles, J., Perestenko, O.V., Bowden, R., Baig, F., Kasten, M., et al. (2019). Single-cell sequencing of iPSC-dopamine neurons reconstructs disease progression and identifies HDAC4 as a regulator of Parkinson cell phenotypes. Cell Stem Cell *24*, 93–106.e6.

Lapasset, L., Milhavet, O., Prieur, A., Besnard, E., Babled, A., Aït-Hamou, N., Leschik, J., Pellestor, F., Ramirez, J.M., De Vos, J., et al. (2011). Rejuvenating senescent and centenarian human cells by reprogramming through the pluripotent state. Genes Dev. *25*, 2248–2253.

Li, H., Jiang, H., Yin, X., Bard, J.E., Zhang, B., and Feng, J. (2019). Attenuation of PRRX2 and HEY2 enables efficient conversion of adult human skin fibroblasts to neurons. Biochem. Biophys. Res. Commun. *516*, 765–769.

Lin, L., Göke, J., Cukuroglu, E., Dranias, M.R., VanDongen, A.M.J., and Stanton, L.W. (2016). Molecular features underlying neurodegeneration identified through in vitro modeling of genetically diverse Parkinson's disease patients. Cell Rep. *15*, 2411–2426.

Luo, S.X., and Huang, E.J. (2016). Dopaminergic neurons and brain reward pathways: from neurogenesis to circuit assembly. Am. J. Pathol. *186*, 478–488.

Mertens, J., Herdy, J.R., Traxler, L., Schafer, S.T., Schlachetzki, J.C.M., Böhnke, L., Reid, D.A., Lee, H., Zangwill, D., Fernandes, D.P., et al. (2021). Age-dependent instability of mature neuronal fate in induced neurons from Alzheimer's patients. Cell Stem Cell *28*, 1533–1548.e6.

Mertens, J., Paquola, A.C.M., Ku, M., Hatch, E., Böhnke, L., Ladjevardi, S., McGrath, S., Campbell, B., Lee, H., Herdy, J.R., et al. (2015). Directly reprogrammed human neurons retain aging-associated transcriptomic signatures and reveal age-related nucleocytoplasmic defects. Cell Stem Cell *17*, 705–718.

Metzakopian, E., Bouhali, K., Alvarez-Saavedra, M., Whitsett, J.A., Picketts, D.J., and Ang, S.L. (2015). Genome-wide characterisation of Foxa1 binding sites reveals several mechanisms for regulating neuronal differentiation in midbrain dopamine cells. Development *142*, 1315–1324.

Miller, J.D., Ganat, Y.M., Kishinevsky, S., Bowman, R.L., Liu, B., Tu, E.Y., Mandal, P.K., Vera, E., Shim, J.w., Kriks, S., et al. (2013). Human iPSC-based modeling of late-onset disease via progerin-induced aging. Cell Stem Cell *13*, 691–705.

Nelander, J., Grealish, S., and Parmar, M. (2013). Human foetal brain tissue as quality control when developing stem cells towards cell replacement therapy for neurological diseases. Neuroreport *24*, 1025–1030.

Park, W.D., O'Brien, J.F., Lundquist, P.A., Kraft, D.L., Vockley, C.W., Karnes, P.S., Patterson, M.C., and Snow, K. (2003). Identification of 58 novel mutations in Niemann-Pick disease type C: correlation with biochemical phenotype and importance of PTC1-like domains in NPC1. Hum. Mutat. *22*, 313–325.

Pereira, M., Pfisterer, U., Rylander, D., Torper, O., Lau, S., Lundblad, M., Grealish, S., and Parmar, M. (2014). Highly efficient generation of induced neurons from human fibroblasts that survive transplantation into the adult rat brain. Sci. Rep. *4*, 6330.

Pfisterer, U., Kirkeby, A., Torper, O., Wood, J., Nelander, J., Dufour, A., Björklund, A., Lindvall, O., Jakobsson, J., and Parmar, M. (2011). Direct conversion of human fibroblasts to dopaminergic neurons. Proc. Natl. Acad. Sci. USA *108*, 10343–10348.

Pircs, K., Nagy, P., Varga, A., Venkei, Z., Erdi, B., Hegedus, K., and Juhasz, G. (2012). Advantages and limitations of different

p62-based assays for estimating autophagic activity in Drosophila. PLoS One *7*, e44214.

Pircs, K., Petri, R., Madsen, S., Brattås, P.L., Vuono, R., Ottosson, D.R., St-Amour, I., Hersbach, B.A., Matusiak-Brückner, M., Lundh, S.H., et al. (2018). Huntingtin aggregation impairs autophagy, leading to argonaute-2 accumulation and global MicroRNA dysregulation. Cell Rep. *24*, 1397–1406.

Poulin, J.F., Zou, J., Drouin-Ouellet, J., Kim, K.Y.A., Cicchetti, F., and Awatramani, R.B. (2014). Defining midbrain dopaminergic neuron diversity by single-cell gene expression profiling. Cell Rep. *9*, 930–943.

Robak, L.A., Jansen, I.E., van Rooij, J., Uitterlinden, A.G., Kraaij, R., Jankovic, J., International Parkinson's Disease Genomics Consortium IPDGC, Heutink, P., and Shulman, J.M. (2017). Excessive burden of lysosomal storage disorder gene variants in Parkinson's disease. Brain *140*, 3191–3203.

Rubinsztein, D.C., Mariño, G., and Kroemer, G. (2011). Autophagy and aging. Cell *146*, 682–695.

Salvador, N., Aguado, C., Horst, M., and Knecht, E. (2000). Import of a cytosolic protein into lysosomes by chaperone-mediated autophagy depends on its folding state. J. Biol. Chem. *275*, 27447–27456.

Sánchez-Danés, A., Richaud-Patin, Y., Carballo-Carbajal, I., Jiménez-Delgado, S., Caig, C., Mora, S., Di Guglielmo, C., Ezquerra, M., Patel, B., Giralt, A., et al. (2012). Disease-specific phenotypes in dopamine neurons from human iPS-based models of genetic and sporadic Parkinson's disease. EMBO Mol. Med. *4*, 380–395.

Schöndorf, D.C., Aureli, M., McAllister, F.E., Hindley, C.J., Mayer, F., Schmid, B., Sardi, S.P., Valsecchi, M., Hoffmann, S., Schwarz, L.K., et al. (2014). iPSC-derived neurons from GBA1-associated Parkinson's disease patients show autophagic defects and impaired calcium homeostasis. Nat. Commun. *5*, 4028.

Shrigley, S., Pircs, K., Barker, R.A., Parmar, M., and Drouin-Ouellet, J. (2018). Simple generation of a high yield culture of induced neurons from human adult skin fibroblasts. J. Vis. Exp. *132*, 56904.

Sposito, T., Preza, E., Mahoney, C.J., Setó-Salvia, N., Ryan, N.S., Morris, H.R., Arber, C., Devine, M.J., Houlden, H., Warner, T.T., et al. (2015). Developmental regulation of tau splicing is disrupted in stem cell-derived neurons from frontotemporal dementia patients with the 10 + 16 splice-site mutation in MAPT. Hum. Mol. Genet. *24*, 5260–5269.

Tang, Y., Liu, M.L., Zang, T., and Zhang, C.L. (2017). Direct reprogramming rather than iPSC-based reprogramming maintains aging hallmarks in human motor neurons. Front. Mol. Neurosci. *10*, 359.

Tiklová, K., Björklund, Å.K., Lahti, L., Fiorenzano, A., Nolbrant, S., Gillberg, L., Volakakis, N., Yokota, C., Hilscher, M.M., Hauling, T., et al. (2019). Single-cell RNA sequencing reveals midbrain dopamine neuron diversity emerging during mouse brain development. Nat. Commun. *10*, 581.

Valenca, G.T., Srivastava, G.P., Oliveira-Filho, J., White, C.C., Yu, L., Schneider, J.A., Buchman, A.S., Shulman, J.M., Bennett, D.A., and De Jager, P.L. (2016). The role of MAPT haplotype H2 and isoform 1N/4R in parkinsonism of older adults. PLoS One *11*, e0157452.

Vuono, R., Winder-Rhodes, S., de Silva, R., Cisbani, G., Drouin-Ouellet, J., REGISTRY Investigators of the European Huntington's Disease Network, Spillantini, M.G., Cicchetti, F., and Barker, R.A. (2015). The role of tau in the pathological process and clinical expression of Huntington's disease. Brain *138*, 1907–1918.

Winder-Rhodes, S.E., Garcia-Reitböck, P., Ban, M., Evans, J.R., Jacques, T.S., Kemppinen, A., Foltynie, T., Williams-Gray, C.H., Chinnery, P.F., Hudson, G., et al. (2012). Genetic and pathological links between Parkinson's disease and the lysosomal disorder Sanfilippo syndrome. Mov. Disord. *27*, 312–315.

Stem Cell Reports, Volume *17*

Supplemental Information

Age-related pathological impairments in directly reprogrammed dopaminergic neurons derived from patients with idiopathic Parkinson's disease

Janelle Drouin-Ouellet, Emilie M. Legault, Fredrik Nilsson, Karolina Pircs, Julie Bouquety, Florence Petit, Shelby Shrigley, Marcella Birtele, Maria Pereira, Petter Storm, Yogita Sharma, Andreas Bruzelius, Romina Vuono, Malin Kele, Thomas B. Stoker, Daniella Rylander Ottosson, Anna Falk, Johan Jakobsson, Roger A. Barker, and Malin Parmar

Supplemental figures and legends

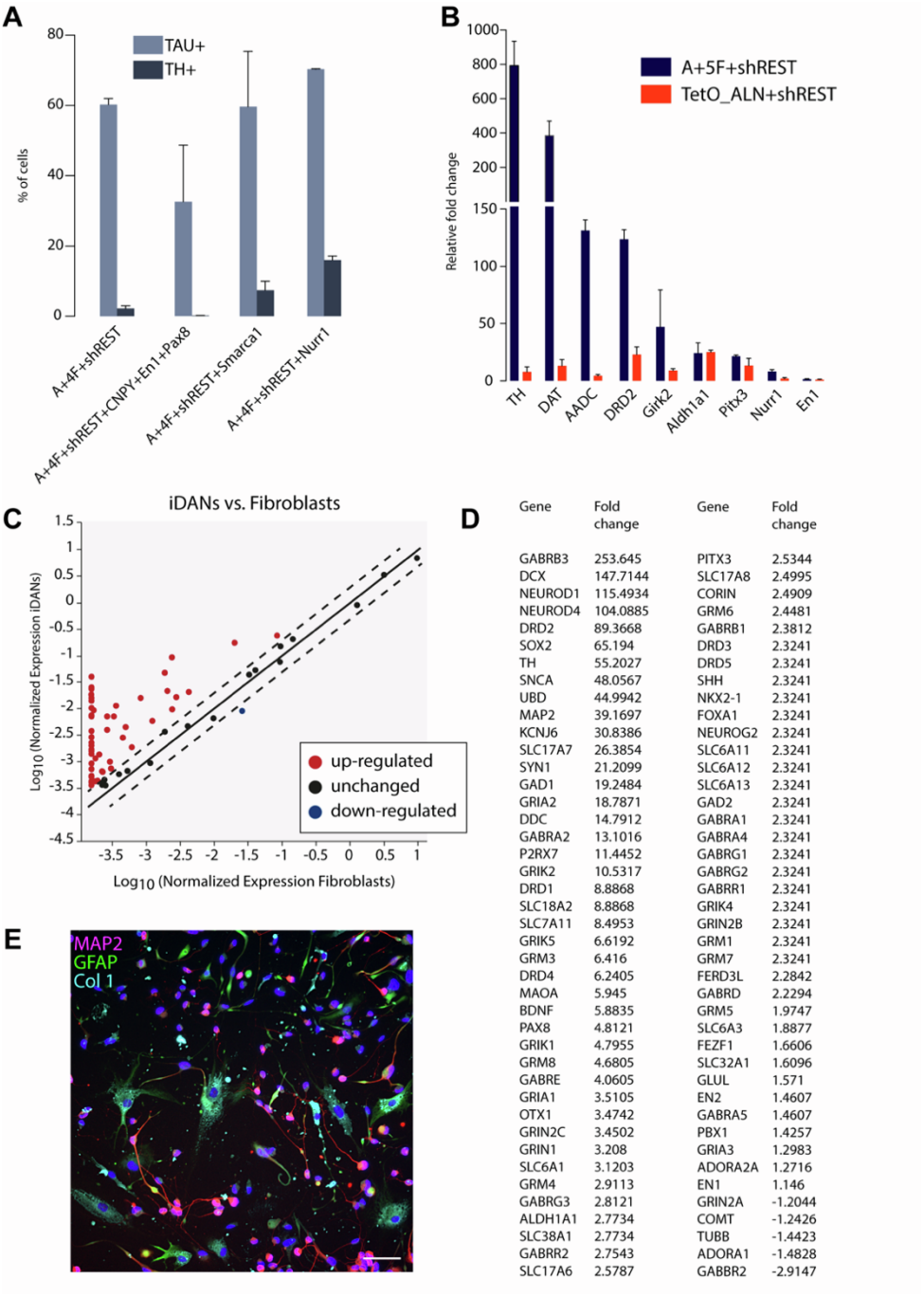

Gene	Fold change	Gene	Fold change
GABRB3	253.645	PITX3	2.5344
DCX	147.7144	SLC17A8	2.4995
NEUROD1	115.4934	CORIN	2.4909
NEUROD4	104.0885	GRM6	2.4481
DRD2	89.3668	GABRB1	2.3812
SOX2	65.194	DRD3	2.3241
TH	55.2027	DRD5	2.3241
SNCA	48.0567	SHH	2.3241
UBD	44.9942	NKX2-1	2.3241
MAP2	39.1697	FOXA1	2.3241
KCNJ6	30.8386	NEUROG2	2.3241
SLC17A7	26.3854	SLC6A11	2.3241
SYN1	21.2099	SLC6A12	2.3241
GAD1	19.2484	SLC6A13	2.3241
GRIA2	18.7871	GAD2	2.3241
DDC	14.7912	GABRA1	2.3241
GABRA2	13.1016	GABRA4	2.3241
P2RX7	11.4452	GABRG1	2.3241
GRIK2	10.5317	GABRG2	2.3241
DRD1	8.8868	GABRR1	2.3241
SLC18A2	8.8868	GRIK4	2.3241
SLC7A11	8.4953	GRIN2B	2.3241
GRIK5	6.6192	GRM1	2.3241
GRM3	6.416	GRM7	2.3241
DRD4	6.2405	FERD3L	2.2842
MAOA	5.945	GABRD	2.2294
BDNF	5.8835	GRM5	1.9747
PAX8	4.8121	SLC6A3	1.8877
GRIK1	4.7955	FEZF1	1.6606
GRM8	4.6805	SLC32A1	1.6096
GABRE	4.0605	GLUL	1.571
GRIA1	3.5105	EN2	1.4607
OTX1	3.4742	GABRA5	1.4607
GRIN2C	3.4502	PBX1	1.4257
GRIN1	3.208	GRIA3	1.2983
SLC6A1	3.1203	ADORA2A	1.2716
GRM4	2.9113	EN1	1.146
GABRG3	2.8121	GRIN2A	-1.2044
ALDH1A1	2.7734	COMT	-1.2426
SLC38A1	2.7734	TUBB	-1.4423
GABRR2	2.7543	ADORA1	-1.4828
SLC17A6	2.5787	GABBR2	-2.9147

Figure S1 related to Figure 1. Generation of iDANs.
(A) Quantification of TAU-positive and TH-positive cells using different reprogramming factors. A: Ascl1, 4F: Lmx1a, Lmx1b, FoxA2, Otx2.
(B) Gene expression quantification of DA genes relative to parental fibroblast levels (from 2 to 3 well replicates). 5F: Lmx1a, Lmx1b, FoxA2, Otx2, Nurr1. TetO_ALN: Ascl1, Lmx1a, Nurr1 from (Caiazzo et al., 2011).
(C) Fold change of all the neuronal and dopaminergic related genes on the qPCR array as compared to parental fibroblasts. Significantly up- and down-regulated genes are in red and blue, respectively.
(D) Fold change of the top up-regulated neuronal, dopaminergic, glutamatergic and GABAergic related genes as compared to parental fibroblasts.
(E) MAP2, GFAP and Collagen 1 expression at 25 days following the start of conversion with the pB.pA.shREST all-in-one vector. Scale bar = 100 μm.

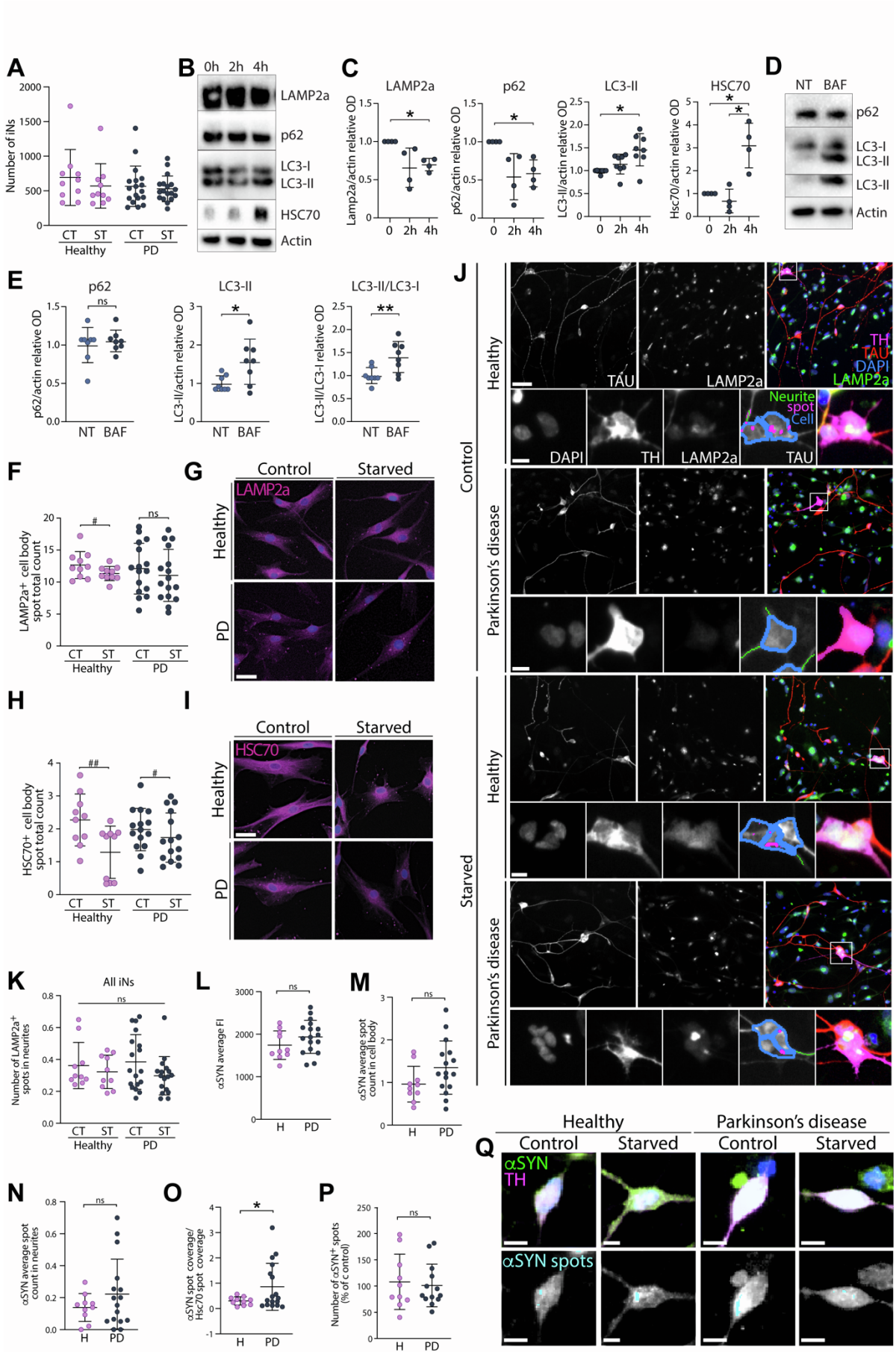
A
Number of iNs
CT ST CT ST
Healthy PD
B
0h 2h 4h
LAMP2a
p62
LC3-I
LC3-II
HSC70
Actin
C
LAMP2a
p62
LC3-II
HSC70
Lamp2a/actin relative OD
p62/actin relative OD
LC3-II/actin relative OD
Hsc70/actin relative OD
0 2h 4h
D
NT BAF
p62
LC3-I
LC3-II
LC3-II
Actin
E
p62
LC3-II
LC3-II/LC3-I
p62/actin relative OD
LC3-II/actin relative OD
LC3-II/LC3-I relative OD
ns
NT BAF
F
LAMP2a+ cell body spot total count
CT ST CT ST
Healthy PD
G
Control Starved
LAMP2a
Healthy
PD
H
HSC70+ cell body spot total count
CT ST CT ST
Healthy PD
I
Control Starved
HSC70
Healthy
PD
J
Control
Starved
Healthy
Parkinson's disease
TAU
LAMP2a
TH
TAU
DAPI
LAMP2a
DAPI
TH
LAMP2a
TAU
Neurite
spot
Cell
K
All iNs
Number of LAMP2a+ spots in neurites
CT ST CT ST
Healthy PD
L
αSYN average FI
H PD
M
αSYN average spot count in cell body
H PD
N
αSYN average spot count in neurites
H PD
O
αSYN spot coverage/ Hsc70 spot coverage
H PD
P
Number of αSYN+ spots (% of c control)
H PD
Q
Healthy
Parkinson's disease
Control
Starved
Control
Starved
αSYN
TH
αSYN spots

Figure S2 related to Figure 2. Chaperone-mediated autophagy impairment in PD-iDANs but not in PD-fibroblasts upon starvation.

(A) Quantification of the number of TAU+ iNs following a 4-hour starvation period.

(B) Representative WB image showing LAMP2a, SQSTM1 (p62), LC3, HSC70 and Actin immunolabeling in iNs from a healthy donor starved for 0, 2 and 4 hours.

(C) OD quantification of LAMP2a, SQSTM1 (p62), LC3, HSC70 immunoblots in iNs starved for 0, 2 and 4 hours. One-way ANOVA on repeated measures, Tukey post-hoc: *p<0.05. Data are shown as mean ± SD. Values were normalized to non-treated expression levels and corrected to actin values.

(D) Representative WB image showing SQSTM1 (p62), LC3 and Actin immunolabeling in non-treated (NT) and Bafilomycin A1 (BAF) treated healthy donor iNs.

(E) OD quantification of p62, LC3 immunoblots in NT and BAF treated healthy donor iNs. Two-tailed unpaired t-test: *P<0.05; **P<0.01. Data are shown as mean ± SD. Values were normalized to non-treated expression levels and corrected to actin values.

(F) Quantification of LAMP2a-positive dots in fibroblasts (mean average of 2,949 cells assessed per line). One-way ANOVA, Bonferroni post-hoc: P=0.59. Paired student's t-test: #P<0.05, as compared to the non-starved condition.

(G) LAMP2a-positive dot expression in fibroblasts. Scale bar = 25µm.

(H) Quantification of HSC70-positive dots in fibroblasts (mean average of 2,949 cells assessed per line). Kruskal-Wallis test, Dunn's multiple comparisons test: P=0.11; H: Wilcoxon matched pairs signed rank test: ##P=0.0098, rs=0.346. PD: Two-tailed paired t-test: #P=0.0406, df=13.

(I) HSC70-positive dot expression and spot detection analysis in fibroblasts. Scale bar = 25µm.

(J) LAMP2a-positive dot expression and spot detection analysis of LAMP2a-positive dots (in pink) in double TAU-positive/TH-positive iDANs. Cell bodies are traced in blue and neurites in green. Scale bar = 50µm; insets = 10µm.

(K) Quantification of LAMP2a-positive dots in neurites of TAU-positive iNs (mean average of 603 iNs assessed per line).

(L) Quantification of αsyn-positive fluorescence intensity in TH-positive iDANs.

(M) Quantification of αsyn-positive spot count in the cell body of TH-positive iDANs.

(N) Quantification of αsyn-positive spot count in the neurites of TH-positive iDANs.

(O) Quantification of αsyn-positive/HSC70 spot coverage in the cell body of TH-positive iDANs. Two-tailed unpaired t-test with Welch's correction: *P=0.0267, df=17.62.

(P) Quantification of αsyn-positive spot count in TH-positive iDANs following starvation.

(Q) αsyn-positive dot expression and spot detection analysis of asyn-positive dots (in cyan) in TH-positive iDANs. Scale bar = 10µm.

Abbreviations: CT: control, H: healthy, ns: not significant, PD: Parkinson's disease, ST: starved.

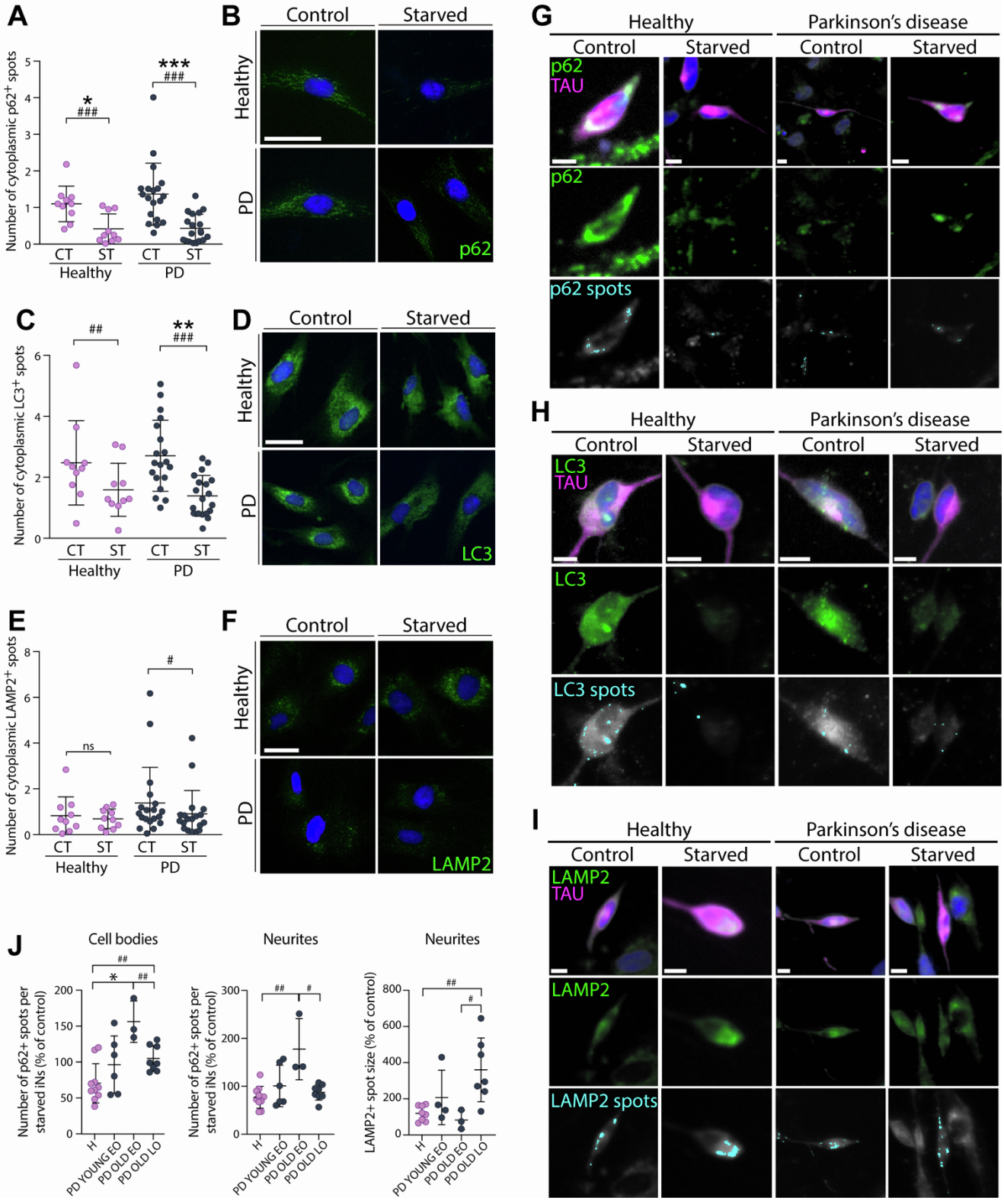
A
Number of cytoplasmic p62+ spots
CT
ST
Healthy
PD
B
Control
Starved
Healthy
PD
p62
C
Number of cytoplasmic LC3+ spots
D
LC3
E
Number of cytoplasmic LAMP2+ spots
ns
F
LAMP2
G
Healthy
Parkinson's disease
p62
TAU
p62 spots
H
LC3
TAU
LC3 spots
I
LAMP2
TAU
LAMP2 spots
J
Cell bodies
Neurites
Number of p62+ spots per starved iNs (% of control)
LAMP2+ spot size (% of control)
H
PD YOUNG EO
PD OLD EO
PD OLD LO

Figure S3 related to Figure 3. P62, LC3 and LAMP2 expression in fibroblasts and iNs vs. iDANs upon starvation.

(A) Quantification of p62-positive dots in fibroblasts (mean average of 625 cells assessed per line). One-way ANOVA, Bonferroni post-hoc: *p<0.05, ***p<0.001. Paired student's t-test: ###p<0.001 as compared to the condition without starvation.

(B) p62-positive dot expression and spot detection analysis in fibroblasts. Scale bar = 25µm

(C) Quantification of LC3-positive dots in fibroblasts (mean average of 651 cells assessed per line). One-way ANOVA, Bonferroni post-hoc: **p<0.01, as compared to the healthy group. Paired student's t-test: ##p<0.01, ###p<0.001 as compared to the condition without starvation.

(D) LC3-positive dot expression and spot detection analysis in fibroblasts. Scale bar = 25µm

(E) Quantification of LAMP2-positive dots in fibroblasts (mean average of 1,126 cells assessed per line). Paired student's t-test: #p<0.05 as compared to the condition without starvation.

(F) LAMP2-positive dot expression and spot detection analysis in fibroblasts. Scale bar = 25µm

(G) p62-positive dot expression in TAU-positive cells. Cyan overlays represent the puncta that were quantified for analysis. Scale bars = 10µm

(H) LC3-positive dot expression in TAU-positive cells. Cyan overlays represents the puncta that were quantified for analysis. Scale bars = 10µm

(I) LAMP2-positive dot expression in TAU-positive cells. Cyan overlays represent the puncta that were quantified for analysis. Scale bars = 10µm

(J) Differences in the number of p62-positive dots per starved iNs in different cell compartments, and of LAMP2+ spot size per neurite depending on the age and age at onset of the PD patient. Young EO: patients younger than 60 years of age, with disease onset before 60 years of age. Old EO: patients older than 60 years of age, with disease onset before 60 years of age. Old LO: patients older than 60 years of age, with disease onset after 60 years of age. Kruskal-Wallis test: *P=0.0106; Unpaired t-test or Mann-Whitney test (depending on the normality of the distribution): #P<0.05, ##P<0.01.

Abbreviations: CT: control, H: healthy, ns: not significant, PD: Parkinson's disease, ST: starved.

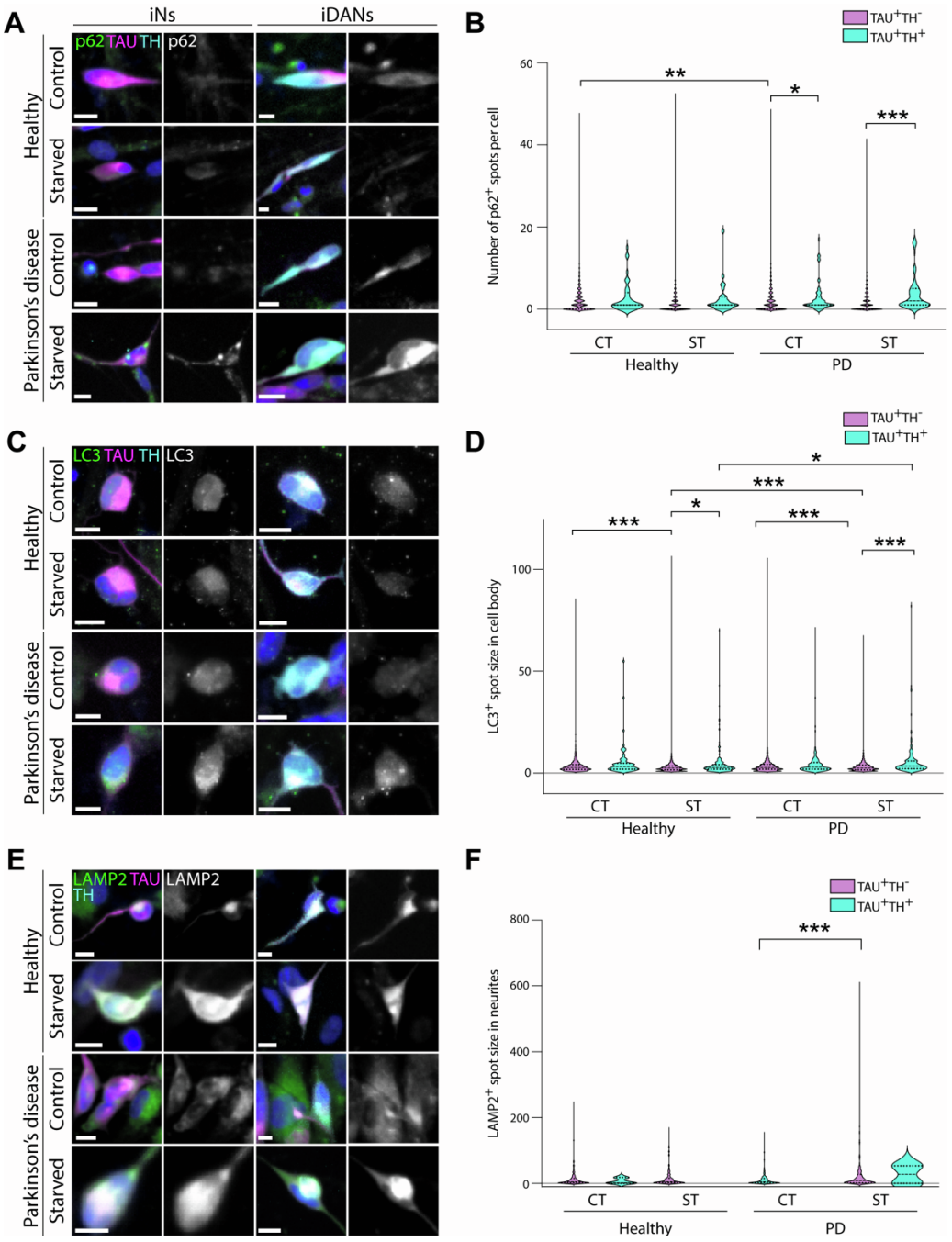

Figure S4 related to Figure 3. p62, LC3 and LAMP2 in iNs vs. iDANs upon starvation.

(A) p62-positive dot expression in TAU-positive/TH-negative and TAU-positive/TH-positive cells. Scale bars = 10μM.

(B) Violin plot showing quantification of p62-positive dots in TAU-positive/TH-negative and TAU-positive/TH-positive cells. Kruskal-Wallis test, Dunn's multiple comparisons test: *p<0.05, **p<0.01, ***p<0.001.

(C) LC3-positive dot expression in TAU-positive/TH-negative and TAU-positive/TH-positive cells. Scale bars = 10μM.

(D) Violin plot showing quantification of LC3-positive dots in TAU-positive/TH-negative and TAU-positive/TH-positive cells. Kruskal-Wallis test, Dunn's multiple comparisons test: *p<0.05, ***p<0.001.

(E) LAMP2-positive dot expression in TAU-positive/TH-negative and TAU-positive/TH-positive cells. Scale bars = 10μM.

(F) Violin plot showing quantification of LAMP2-positive dots in TAU-positive/TH-negative and TAU-positive/TH-positive cells. Kruskal-Wallis test, Dunn's multiple comparisons test: ***p<0.001.

Abbreviations: CT: control, H: healthy, PD: Parkinson's disease, ST: starved.

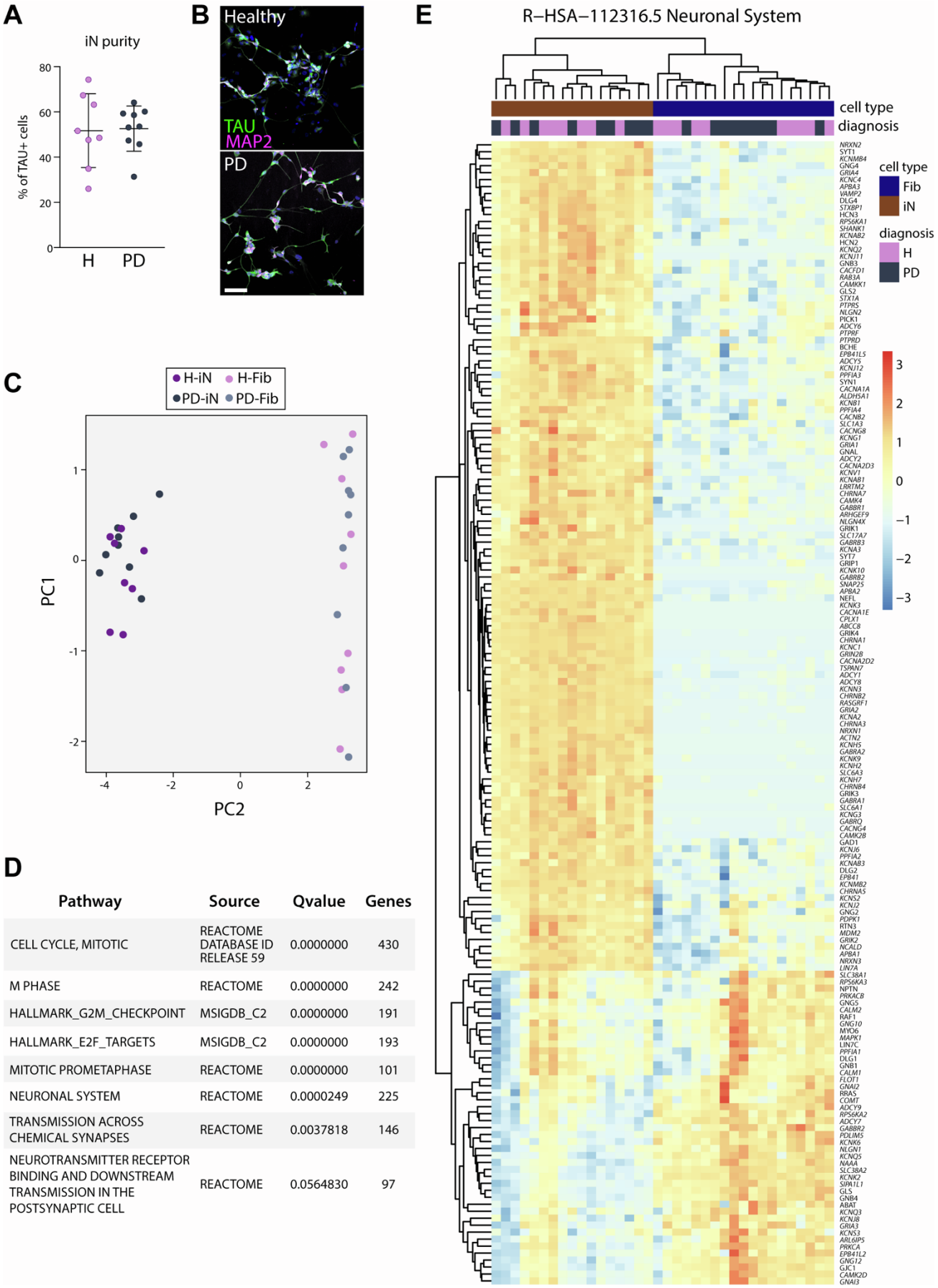

D

Pathway	Source	Qvalue	Genes
CELL CYCLE, MITOTIC	REACTOME DATABASE ID RELEASE 59	0.0000000	430
M PHASE	REACTOME	0.0000000	242
HALLMARK_G2M_CHECKPOINT	MSIGDB_C2	0.0000000	191
HALLMARK_E2F_TARGETS	MSIGDB_C2	0.0000000	193
MITOTIC PROMETAPHASE	REACTOME	0.0000000	101
NEURONAL SYSTEM	REACTOME	0.0000249	225
TRANSMISSION ACROSS CHEMICAL SYNAPSES	REACTOME	0.0037818	146
NEUROTRANSMITTER RECEPTOR BINDING AND DOWNSTREAM TRANSMISSION IN THE POSTSYNAPTIC CELL	REACTOME	0.0564830	97

Figure S5 related to Figure 5. iN transcription profile.
(A) Quantification of the TAU-positive cell purity from a well replicate of the cells sent for RNA-seq (mean average of 16,221 cells assessed per line).
(B) Double TAU-positive and MAP2-positive iNs from a well replicate of the cells sent for RNA-seq. Scale bar = 100µm.
(C) Principal component analysis showing a separation of the reprogrammed iNs from the parental fibroblasts on PC2.
(D) Gene set enrichment analysis showing top eight most up and down regulated pathways in iNs compared to fibroblasts.
(E) Hierarchical clustering of RNA-seq samples, using Euclidean distance on normalized and log2-transformed read counts.
Abbreviations: Fib: fibroblasts; H: healthy, iN: induced neurons; PD: Parkinson's disease.

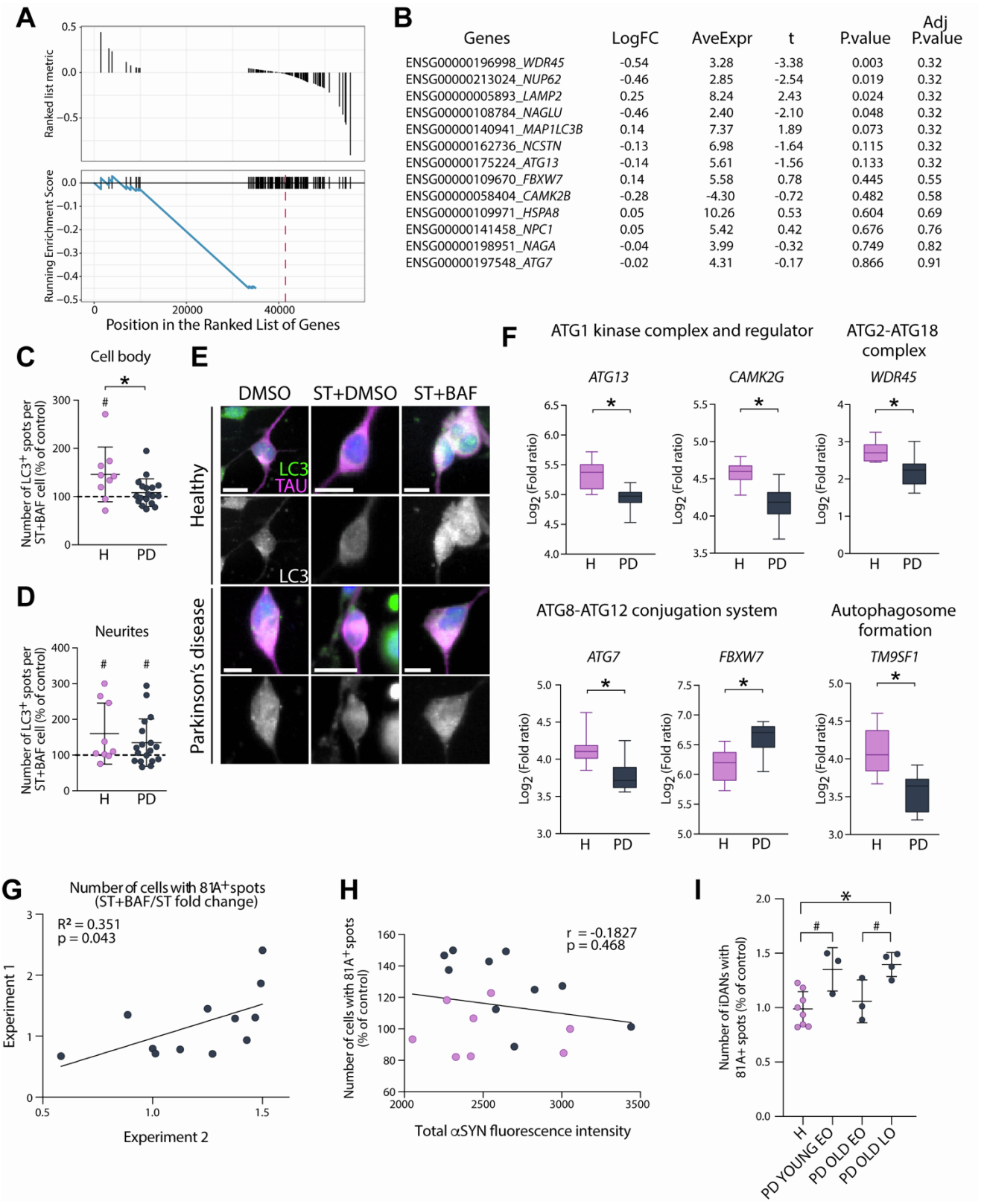

Figure S6 related to Figures 5 and 6. PD-iNs do not accumulate autophagosome structures following impairment of autophagy but accumulate phosphorylated aSYN.

(A) GSEA plot of the "LYSOSOME" KEGG pathway in PD-iNs (Adj.P.Val = 0.028).

(B) LogFC and P. value table of autophagy and lysosome related genes in parental fibroblasts. Negative logFC means down-regulated in PD. Adj.P.Val" represents the P.value after transcriptome wide adjustment with the FDR method. (n=10 healthy and n=10 PD lines).

(C) Quantification of LC3-positive puncta in the cell body of TAU-positive iNs (mean average of 425 TAU-positive cells assessed per line, n=9 healthy and n=18 PD lines). Kolmogorov-Smirnov test: *P=0.0493, D=55.56. Two-tailed Wilcoxon matched pairs signed rank test, #P=0.0371.
(D) Quantification of LC3-positive puncta in the neurites of TAU-positive iNs (mean average of 425 TAU-positive cells assessed per line, n=9 healthy and n=18 PD lines). H: two-tailed Wilcoxon matched pairs signed rank test, #P=0.0371, PD: two-tailed paired t-test: #P=0.0499, df=16.
(E) LC3-positive dot expression and spot detection analysis in TAU-positive iNs. Scale bar = 10µm.
(F) Boxplots of $\log_2$ fold changes in expression of genes associated with autophagy (n=10 healthy and n=10 PD lines) (adjusted P value < 0.05).
(G) Reproducibility of the experiment shown in Figure 6C,D as assessed by a positive correlation between the number of iNs with 81A-positive puncta between two independent experiments (different lentiviral batches, passage number of the parental fibroblasts, laboratory in which they were done as well as the experimenter performing the experiments and the quantifications), showing that the same cell line show 81A-positive puncta accumulation independently of the experimental conditions. Pearson's correlation: P=0.043; 95% confidence interval: 0.02770 to 0.8703.
(H) No association between the number of 81A-positive puncta and the total asyn fluorescence intensity in iDANs (n=18 lines). Spearman's rank correlation: P=0.468; 95% confidence interval: -0.6080 to 0.3242.
(I) Differences in the number of iDANs with 81A-positive puncta depending on the age of the PD patient and their age at onset. Young EO: patients younger than 60 years of age, with disease onset before years of age. Old EO: patients older than 60 years of age, with disease onset before 60 years of age. Old LO: patients older than 60 years of age, with disease onset after 60 years of age. One-way ANOVA: *P =0.0458. Unpaired t-test: #P<0.05.

Supplemental Table

Table S1. List of Antibodies

Antibody	Source	Species	Dilution	Catalogue number	Antibody registry number or PMIDs
81A	Gift from Kelvin Luk, University of Pennsylvania	Mouse	1:10 000	NA	24931606, 24659240, 25732816
	Abcam	Mouse	1:500	Ab184674	AB_2819037
Alpha-synuclein	Abcam	Chicken	1:1 000	Ab190376	AB_2747764
Aldh1a1	Abcam	Rabbit	1:200	Ab23375	AB_2224009
Collagen 1	Abcam	Rabbit	1:1 000	Ab34710	AB_731684
GFAP	Millipore	Mouse	1:1 000	MAB3402	AB_94844
Anti-Histone H2A.X, phospho (Ser139)	Millipore	Mouse	1:500	05-636	AB_309864
HSC70	Abcam	Rat	ICC: 1:2 000 WB: 1:5 000	Ab19136	AB_444764
	Thermo Scientific	Mouse	1:100	MA3-014	AB_325462
LAMP2	DSHB	Mouse	1:100	H4B4	AB_528129
LAMP2a	Abcam	Rabbit	ICC: 1:1 000 WB: 1:2 000	Ab18528	AB_775981
LC3B	Sigma	Rabbit	ICC: 1:500 WB: 1:5 000	L7543	AB_796155
MAP2	Abcam	Chicken	1:10 000	Ab5392	AB_2138153
P62	Abcam	Rabbit	ICC: 1:500 WB: 1:5 000	Ab91526	AB_2050336
TAU HT7	Thermo Fisher Scientific	Mouse	1:500	MN1000	AB_2314654
TAU	Agilent Technologies	Rabbit	1:500	A0024	AB_10013724
TH	Millipore	Sheep	1:1 000	Ab1542	AB_90755
VMAT2	Sigma	Rabbit	1:200	AB1598P	AB_2285927

Supplemental experimental procedures

Genotyping and DNA-sequencing

All patients were screened for three common Mendelian mutations associated with late onset PD: *LRRK2 G2019S* as well as *GBA L444P* and *GBA N370S*. One out of 19 patients was identified as a *LRRK2 G2019S* mutation carrier and was removed from further analysis. Samples were also screened for SNCA gene expression levels in our RNA-seq dataset to detect any overexpression of the *SNCA* gene in the iN samples that would suggest a duplication or triplication. All PD samples included in the RNA-seq analysis had *SNCA* expression that followed a normal distribution without any outliers. For *MAPT* haplotype genotyping, single nucleotide polymorphism (SNP) genotyping was undertaken using a predesigned assay, rs9468 (Applied Biosystems), tagging the *MAPT H1* versus *H2* haplotype, and run on a Quantstudio 7 Flex Real-Time PCR System (ThermoFisher), according to the manufacturer's instructions. There were no inconsistencies amongst the 28 samples genotyped in triplicates.

Cell culture

Fibroblasts were expanded in T75 flasks with standard fibroblast medium (DMEM, 10 % FBS, 100U/mL penicillin-streptomycin) at 37°C in 5 % CO_2. After thawing, cells were kept for a minimum of two days in culture before starting experiments. When confluent, the cells were dissociated with 0.05 % trypsin and plated at a lower density to expand them. To freeze the fibroblasts from a confluent T75 flask, the cells were detached after 5 minutes incubation in 0.05 % trypsin at 37°C, spun for 5 minutes at 400 g and frozen in a 50/50 mixture of DMEM and FBS with 10 % DMSO. All cell lines were routinely tested for mycoplasma and were negative. For analyses on fibroblasts, cells were plated at a density of 1,900-3,800 cells per cm^2 in 24-well plates (Nunc) and analyses were performed three days later.

Viral vectors and virus transduction

DNA plasmids expressing mouse open reading frames (ORFs) for *ASCL1, LMX1A, LMX1B, FOXA2, OTX2, NURR1, SMARCA1, CNPY, EN1* or *PAX8* in a third-generation lentiviral vector containing a non-regulated ubiquitous phosphoglycerate kinase (PGK) promoter were generated, as well as two short hairpin RNAs (shRNAs) targeting RE1-silencing Transcription Factor (*REST*) containing a non-regulated U6 promoter. Plasmids used in this study have been deposited in Addgene (#33013, #33014, #34997, #35000, #35001, #127573, #127574). Furthermore, the pB.pA.shREST all-in-one vector from (Birtele et al., 2019; Drouin-Ouellet et al., 2017; Shrigley et al., 2018) was used to reprogram iNs for RNA-seq and WB. All the constructs have been verified by sequencing. Lentiviral vectors were produced as previously described (Zufferey et al., 1997) and titrated by qPCR analysis (Georgievska et al., 2004). Transduction was performed at a MOI of 5 for each vector (all viruses used in this study were titered between 1 x 10^8 and 9 x 10^9) or MOI of 20 in the case of the pB.pA.shREST vector.

Fibroblast reprogramming to iPSCs

Fibroblasts were cultured in IMDI medium with 10% FBS and 100U/mL penicillin-streptomycin. Fibroblasts were passaged as single cells using TrypLE Select and seeded at a density of 8,000-15,000 cells/cm^2 on Laminin-521 coated cell culture plates in fibroblast medium. Medium was replaced by Essential E8 medium with 100 U/mL penicillin-streptomycin the day after seeding and thereafter only cultured with E8 medium. Fibroblasts were reprogrammed by using the ReproCELL, StemRNA reprogramming kit. In short, transfection was performed by mixing Lipofectamine RNAiMAX and RNAs provided in the StemRNA kit. Transfection was performed on the hour every 24 hours for four sequential days. Medium was replaced daily, at a minimum 4 hours before transfection. iPSC colonies emerged around day 12-25 post reprogramming and were manually picked for the first passage. Each picked colony was further passaged on as single cells using TrypLE Select. ROCKi at a concentration of 10 µM was added to the Essential 8 medium at each passage. Medium was replaced daily. Quality controls of the generated iPSC colonies were performed from passages 5 and onwards.

Flow analysis

iPSCs were passaged as single cells using TrypLE Select. iPSCs were counted and 200,000-400,000 cells were used for each antibody staining. iPSCs were fixed and permeabilized using the Fixation and Permeabilization buffers according to manufactures instruction (ThermoFisher 00-5523-00). All incubations, fixations and permeabilizations were performed at room temperature. Incubation with antibodies at a concentration of 1 µl/100,000 cells was performed for 30 minutes, at room temperature in the dark. Antibodies provided to separate tubes and unstained cells (without antibody added), were used as negative control. Cells were washed once using Stain buffer before diluted to a concentration of 1 million cell/mL in Stain buffer and passed through a cell strainer before proceeding to Flow analysis. 10,000 events were recorded for each antibody.

Whole cell patch clamp recordings

Cells used for electrophysiological recordings were directly plated onto glass coverslips coated with PFL as described in (Shrigley et al., 2018). Prior to recording, the cells on the coverslips were transferred from the culture medium to BrainPhys medium (Bardy et al., 2015) for 30 minutes and maintained at 34.5 °C. Cells were then moved to a recording chamber and submerged in a flowing artificial cerebrospinal fluid (ACSF) solution gassed with 95 % O_2 and 5 % CO_2. The composition of the ACSF was (in mM): 126 NaCl, 2.5 KCl, 1.2 NaH_2PO_4-H_2O, 1.3 $MgCl_2$-$6H_2O$, and 2.4 $CaCl_2$-$6H_2O$, 22 $NaHCO_3$, 10 glucose adjusted to pH = 7.4. Temperature of the chamber was maintained at 34 °C throughout the entire recording session. Multi-clamp 700B (Molecular Devices) was used for the recordings and signals were acquired at 10 kHz using pClamp10 software and a data acquisition unit (Digidata 1440A, Molecular Devices). Current was filtered at 0.1 Hz and digitized at 2 kHz. Borosilicate glass pipettes ranging between 4-7 MΩ were used and they were filled with the following intracellular solution (in mM): 122.5 potassium gluconate, 12.5 KCl, 0.2 EGTA, 10 Hepes, 2 MgATP, 0.3 Na_3GTP and 8 NaCl adjusted to pH = 7.3 with KOH as in (Pfisterer et al., 2011). The intracellular solution was kept on ice during the recordings. Cells with neuronal morphology characterized by a rounded cell body were selected for recordings. Input resistances and injected currents were monitored throughout the experiments. Passive properties of the membrane were monitored, and recordings were discarded when changes in the capacitance were higher than 20 % from the beginning to the end of the recording session. Resting membrane potentials were monitored immediately after breaking-in, in current-clamp mode. The membrane potential was kept between -40 mV to -60 mV and currents were injected for 500 ms from -20 pA to +90 pA with 10 pA increments to induce action potentials. The number of action potentials for each cell was taken as the highest frequency of action potential induced by a step of current within the same cell and averaged over the total cells patched per line. Voltage ramp was characterized by constant increase in voltage from -70 mV to +20 mV in 0.5 sec intervals. Inward sodium and delayed rectifying potassium currents were measured in voltage clamp at depolarizing steps of 10 mV for 100 ms. Spontaneous firing was recorded in voltage-clamp mode at resting membrane potentials. For stem cell-derived iDANs, cells on coverslips were transferred directly to recording chamber with flowing ACSF kept at 34 °C. Membrane potential was kept between -60 mV and -70 mV and currents were injected for 500 ms from -20 pA to +40 pA with 5 pA increments to induce action potentials.

Western blots

Cells were lysed and homogenized as described elsewhere (Pircs et al., 2018). Protein concentration was determined using a DC protein assay kit (Bio-Rad, 5000116). 10-15 µg of protein was boiled at 95°C for 5 min in Laemmli buffer (Bio-Rad), separated on a 4–12 % SDS/PAGE gel and then transferred using the Transblot®-Turbo™ Transfer system (Bio-Rad). After 1 hour blocking in Tris-buffered saline (TBS; 50 mM Tris-Cl, 150 mM NaCl, pH 7.6) with 0.1 % Tween 20 (Sigma-Aldrich, P7949) and 2.5 % (wt:vol) non-fat dry milk (Bio-Rad Laboratories), membranes were incubated overnight at 4°C in one of the primary antibodies summarized in **Table S1**. After washing with TBST, membranes were incubated for 1 hour at room temperature with HRP-conjugated secondary antibodies. Protein expression was developed with the ECL™ Prime Western Blotting Detection Reagent (Life Technologies, RPN2232). Signal was captured using a Chemidoc MP system (Bio-Rad). Band intensity was quantified using ImageJ software (ImageJ, 1.48v) by densitometry.

Immunocytochemistry and high content screening quantifications

Following fixation in 4 % paraformaldehyde, cells were permeabilized with 0.1 % Triton-X-100 in 0.1 M PBS for 10 minutes. Thereafter, cells were blocked for 30 minutes in a solution containing 5 % normal serum in 0.1 M PBS. The primary antibodies were diluted in the blocking solution and applied overnight at 4 °C. Fluorophore-conjugated secondary antibodies (1:200; Jackson ImmunoResearch Laboratories) as well as 4',6-diamidino-2-phenylindole (DAPI; 1:1,000, Sigma Aldrich) were diluted in blocking solution and applied for 2 hours. Fluorescence images of the Heat shock cognate 71 kDa protein (HSC70, also known as HSPA8), lysosome-associated membrane protein 2a (LAMP2a) and tyrosine hydroxylase (TH) and the TAU-81A stainings were taken using a confocal laser scanning microscope (Leica, TCS SP8), whereas the rest of the images were taken using either an inverted microscope (Leica, DFC360 FX-DMI 6000B) or CellInsight CX5 or CX7 High-Content Screening (HCS) microscopes (Thermo Scientific).

The total number of DAPI-positive, TAU-positive and TH-positive cells per well, as well as the average fluorescence intensity for aSYN was quantified using the Cellomics Array Scan (Array Scan VTI, Thermo Fischer), which is an automated process ensuring unbiased measurements between groups. Applying the program "Target Activation", 100-200 fields (10 X magnification) were acquired in a spiral fashion starting from the center, with focus performed on every field of views. The same array, run at 20 X magnification, was used for the analysis of the number of neurites per TAU-positive cell using the program "Neuronal Profiling". Neuronal purity was calculated as the number of TAU- or MAP2-positive cells over the total number of cells in the well at the end of the experiment. Dopaminergic subtype purity was calculated as the number of TH- or aldehyde dehydrogenase 1 family member A1 (ALDH1A1)-positive cells over the total number of TAU- or MAP2-positive cells in the well at the end of the experiment. Average dot number and size was measured in those neurons in which the cytoplasm and neurites were defined by TAU or TH staining. Puncta of p62, LC3, LAMP2, LAMP2a, HSC70, aSYN and 81A were detected (using a "Spot Detection" program) and measured in each case. For each neuron identified by the software based on TAU/MAP2 and TH expression, the number and size of puncta in the cell body and neurites were measured using an isodata thresholding method. The data is presented as the average number or size of dots detected per cell in each compartment. Experiments done on fibroblasts were quantified using the same approach, with quantification of puncta of p62, LC3, LAMP2, LAMP2a and HSC70 in the cytoplasm, defined by vimentin (VIM)-positive staining. For gH2AX measurements, puncta positive for gH2AX were detected in the nuclei of fibroblasts and iDANs (defined by the DAPI stained region) at 20 X magnification using a "Spot Detection" program.

qRT-PCR for neuronal gene expression

Total RNA was extracted from human fibroblasts as well as iNs from the same lines using the miRNeasy kit (Qiagen) followed by Universal cDNA synthesis kit (Fermentas). Three reference genes were used for each qPCR analysis (*ACTB*, *GAPDH* and *HPRT1*). All primers were used together with LightCycler 480 SYBR Green I Master (Roche). Standard procedures of qRT-PCR were used, and data quantified using the ΔΔCt-method. Statistical analyses were performed on triplicates. A custom RT^2 profiler PCR Array (Qiagen) containing 90 neuronal genes was also used according to the manufacturer instructions.

RNA-seq analysis

Fibroblasts from the healthy donor (n = 10) and PD (n = 10) lines were plated and either collected for RNA extraction following 3 days in culture or transduced with the pB.pA.shREST lentiviral vector (Birtele et al., 2019; Drouin-Ouellet et al., 2017; Shrigley et al., 2018) the day following plating and allowed to be reprogrammed for 30 days. RNA was extracted using the RNeasy mini kit (Qiagen) with DNase treatment. cDNA libraries were prepared using the Illumina truseq library preparation kit and sequenced with 2 x 150 bp paired end reads on an Illumina NextSeq 500 High Output kit. For iPSC-iDANs cDNA libraries were generated using Smart-seq2 (Takara). Raw base calls were demultiplexed and converted into sample specific fastq format files using default parameters of the bcl2fastq program provided by illumina. Quality of reads was checked using FastQC and multiQC tools. Reads were mapped to the human genome (GRCh37) using the STAR mapping algorithm (Dobin et al., 2013). mRNA expression was quantified using RSEM (Li and Dewey, 2011). Downstream analyses were performed using in

house R scripts. Gene Set Enrichment Analysis was performed by fitting a linear model, adjusting for sex and disease status as covariates, and genes were ranked based on their association with age at sampling. Six gene sets related to aging were extracted from the gene ontology database and queried using GSEA (as implemented in the clusterProfiler R package). Differential splicing of the *MAPT* gene was visualized in IGV (version 2.8). Significant up and down regulated pathways were selected using Bonferroni post hoc corrected p values (padj < 1e-4).

References

Bardy, C. et al. (2015). Neuronal medium that supports basic synaptic functions and activity of human neurons in vitro. Proc Natl Acad Sci U S A *112*, E2725-34.

Birtele, M., Sharma, Y., Kidnapillai, S., Lau, S., Stoker, T. B., Barker, R. A., Rylander Ottosson, D., Drouin-Ouellet, J., and Parmar, M. (2019). Dual modulation of neuron-specific microRNAs and the REST complex promotes functional maturation of human adult induced neurons. FEBS Lett *593*, 3370-3380.

Caiazzo, M. et al. (2011). Direct generation of functional dopaminergic neurons from mouse and human fibroblasts. Nature *476*, 224-227.

Dobin, A., Davis, C. A., Schlesinger, F., Drenkow, J., Zaleski, C., Jha, S., Batut, P., Chaisson, M., and Gingeras, T. R. (2013). STAR: ultrafast universal RNA-seq aligner. Bioinformatics *29*, 15-21.

Drouin-Ouellet, J. et al. (2017). REST suppression mediates neural conversion of adult human fibroblasts via microRNA-dependent and -independent pathways. EMBO Mol Med *9*, 1117-1131.

Georgievska, B., Jakobsson, J., Persson, E., Ericson, C., Kirik, D., and Lundberg, C. (2004). Regulated delivery of glial cell line-derived neurotrophic factor into rat striatum, using a tetracycline-dependent lentiviral vector. Hum Gene Ther *15*, 934-944.

Li, B., and Dewey, C. N. (2011). RSEM: accurate transcript quantification from RNA-Seq data with or without a reference genome. BMC Bioinformatics *12*, 323.

Pfisterer, U., Kirkeby, A., Torper, O., Wood, J., Nelander, J., Dufour, A., Bjorklund, A., Lindvall, O., Jakobsson, J., and Parmar, M. (2011). Direct conversion of human fibroblasts to dopaminergic neurons. Proc Natl Acad Sci U S A *108*, 10343-10348.

Pircs, K. et al. (2018). Huntingtin Aggregation Impairs Autophagy, Leading to Argonaute-2 Accumulation and Global MicroRNA Dysregulation. Cell Rep *24*, 1397-1406.

Shrigley, S., Pircs, K., Barker, R. A., Parmar, M., and Drouin-Ouellet, J. (2018). Simple Generation of a High Yield Culture of Induced Neurons from Human Adult Skin Fibroblasts. J Vis Exp 56904.

Zufferey, R., Nagy, D., Mandel, R. J., Naldini, L., and Trono, D. (1997). Multiply attenuated lentiviral vector achieves efficient gene delivery in vivo. Nat Biotechnol *15*, 871-875.